CITATIONS

Adler, D. (2009), rgl, R package version 0.84, URL http://rgl.neoscientists.org/about.shtml.

Bailey, T. C., and Gatrell, A. C. (1995), *Interactive Spatial Data Analysis*, San Francisco, CA: Prentice-Hall Inc.

Batschelet, E. (1981), *Circular Statistics in Biology*, London: Academic Press.

Besag, J. (1974), "Spatial Interaction and the Statistical Analysis of Lattice Systems," *Journal of the Royal Statistical Society*, Series B (Methodological), 36(2), 192-236.

Boogaart, K. G. v. d., and Schaeben, H. (2002a), "Kriging of Regionalized Directions, Axes, and Orientations I: Directions and Axes," *Mathematical Geology,* 34(5), 479-503.

— (2002b), "Kriging of Regionalized Directions, Axes, and Orientations II: Orientations," *Mathematical Geology,* 34(6), 671-677.

Brewer, C. A. (1994), "Color Use Guidelines for Mapping and Visualization," in *Visualization in Modern Cartography*, eds. A. M. MacEachren and D. R. F. Taylor, Tarrytown, NY: Elsevier Science, 123-147.

— (1997), "Spectral Schemes: Controversial Color Use on Maps," *Cartography and Geographic Information Systems,* 24(4), 203-220.

Brown, A. J. (2003), URL http://www.aerospaceweb.org/question/spacecraft/q0127a.shtml.

Carr, D. B., Littlefield, R. J., Nicholson, W. L., and Littlefield, J. S. (1987), "Scatterplot Matrix Techniques for Large N," *Journal of the American Statistical Association,* 82(398), 424-436.

CEI (2008), Ensight, URL http://www.ensight.com/visualization.html.

Edwards, C. H., and Penney, D. E. (1988), *Elementary Linear Algebra*, Englewood Cliffs, NJ: Prentice-Hall Inc.

Eisen, M. B., Spellman, P. T., Brown, P. O., and Botstein, D. (1998), "Cluster Analysis and Display of Genome-Wide Expression Patterns," in *Proceedings of the National Academy of Sciences of the United States of America,* 95(25), 14863-14868.

Fisher, N. I. (1993), *Statistical Analysis of Circular Data*, Cambridge: Cambridge University Press.

FLUENT (2008), URL http://www.fluent.com/software/fluent/index.htm.

Foley, J. D., van Dam, A., Feiner, S. K., and Huges, J. F. (1992), *Computer Graphics: Principles and Practice* (2nd ed.), Reading, MA: Addison-Wesley.

Furrer, R., Nychka, D., and Sain, S. (2009), fields, R package version 5.02, URL http://www.image.ucar.edu/GSP/Software/Fields/.

Gneiting, T., and Schlather, M. (2004), "Statistical modeling with covariance functions," In preparation.

Grossman, S. I. (1988), *Calculus* (4th ed.), San Diego, CA: Harcourt Brace Jovanovich, 715-718.

Ihaka, R. R. (2003), "Colour for Presentation Graphics," in *Proceedings of the 3rd International Workshop on Distributed Statistical Computing* (DSC 2003), March 20–22, Vienna, Austria, URL http://www.ci.tuwien.ac.at/Conferences/DSC-2003/Proceedings/Ihaka.pdf.

Ihaka, R. R., and Gentleman, R. (1996), "R: A Language for Data Analysis and Graphics," *Journal of Computational and Graphical Statistics,* 3(5), 299-314.

Ihaka, R. R., Murrell, P., Hornik, K., and Zeileis, A. (2009), colorspace, R package version 1.0-1.

Intelligent Light (2008), FIELDVIEW, URL http://www.ilight.com/products.php.

Jammalamadaka, S. R., and SenGupta, A. (2001), *Topics in Circular Statistics*, Singapore: World Scientific.

Johnson, N. L., Kotz, S., and Balakrishnan, N. (1994), *Continuous Univariate Distributions* (Vol. 1, 2nd ed.), New York: John Wiley and Sons, 327-329.

Jupp, P. E., and Mardia, K. V. (1989), "A Unified View of the Theory of Directional Statistics, 1975-1989," *International Statistical Review,* 57(3), 261-294.

Kosara, K., Healey, C. G., Interrante, V., Laidlaw, D. H., and Ware, C. (2003), "Thoughts on User Studies: Why, How, and When," *IEEE Computer Graphics & Applications (CG&A), Visualization Viewpoints*, 23(4), 20–25, URL http://kosara.net/papers/Kosara_CGA_2003.pdf.

Kovach Computing (2004), Oriana 2, URL http://www.kovcomp.co.uk/oriana/oribroc.html.

Lantuejoul, C. H. (2002), *Geostatistical simulation*, New York: Springer.

Lévy, P. (1939), "L'Addition des Variable Aléatoires Définies sur une Circonférence," *Bulletin de la Société Mathématique de France,* 67, 1-41.

Lund, U. J., and Agostinelli, C. (2007), CircStats, R package version 0.2-3.

Mardia, K. V. (1972), *Statistics of Directional Data*, London: Academic Press.

Mardia, K. V., and Jupp, P. E. (2000), *Statistics of Directional Data*, New York: John Wiley & Sons.

McNeill, L. (1993), "Interpolation and Smoothing of Mapped Circular Data," *South African Statistical Journal,* 27, 23-49.

Minnotte, M. C., and West, R. W. (1998), "The Data Image: A Tool for Exploring High Dimensional Data Sets," in *Proceedings of the American Statistical Association Section on Statistical Graphics*, Alexandria, VA, 25-33, URL http://www.math.usu.edu/~minnotte/research/pubs.html.

Pisces Conservation Ltd (2003), Axis, URL http://www.pisces-conservation.com/index.html?softaxis.html$softwaremenu.html.

Press, W. H., Flannery, B. P., Teukolsky, S. A., and Vetterling, W. T. (1986), *Numerical Recipes, the Art of Scientific Computing*, Cambridge: Cambridge University Press.

Quimby, W. F. (1986), "Selected Topics in Spatial Statistical Analysis: Non-Stationary Vector Kriging, Large Scale Conditional Simulation of Three Dimensional Gaussian Random Fields, and Hypothesis Testing in a Correlated Random Field," unpublished PhD Thesis, University of Wyoming, Laramie: Coe Library Microfilm.

R Development Core Team (2008), R: A Language and Environment for Statistical Computing, R Foundation for Statistical Computing, Vienna, Austria, ISBN 3-900051-07-0, URL http://www.r-project.org/.

Rencher, A. C. (1975), *Statistics 522, Introduction to Linear Models* (1st ed.), Provo, UT: Brigham Young University, 4-75 45 12336.

Ribeiro Jr., P. J., and Diggle, P. J. (2001), "geoR: A Package for Geostatistical Analysis," *R News*, 1(2), 15-17, URL http://www.est.ufpr.br/geoR.

Rice, J. A. (1995), *Mathematical Statistics and Data Analysis* (2nd ed.), Belmont, CA: Duxbury Press.

Schaeben, H., Boogaart, K. G. v. d., and Apel, M. (2001), "Kriging of Surface Normal Vectors," CD-ROM in *Proceedings of 2001 Annual Conference of the International Association for Mathematical Geology*, September 6-12, Cancun, Mexico.

Schlather, M. (1999), "Introduction to Positive Definite Functions and to Unconditional Simulation of Random Fields," Technical Report ST-99-10, Department of Mathematics and Statistics, Faculty of Applied Sciences, Lancaster University, UK.

— (2001), "Simulation and Analysis of Random Fields," *R News*, 1(2), 18-20.

Scientific Software Group (2008), Surfer 8, URL http://www.ssg-surfer.com/html/surfer_details.html.

Seber, G. A. F. (1977), *Linear Regression Analysis*, New York: John Wiley and Sons.

Wand, M. P., and Jones, M. C. (1995), *Kernel Smoothing*, London: Chapman and Hall.

Ware, C. (2004), *Information Visualization* (2nd ed.), San Francisco: Morgan Kaufmann.

Watson, G. S., and Williams, E. J. (1956), "On the Construction of Significance Tests on the Circle and the Sphere," *Biometrika,* 43(3/4), 344-352.

Weast, R. C. (1972), *Handbook of Chemistry and Physics* (53rd ed.), Cleveland, OH: CRC Press.

Worsley, K. J. (2002), "Random Field, Gaussian," standard article in *Encyclopedia of Environmetrics*, eds. A.H. El-Shaarawi and W.W. Piegorsch, Chichester, NY: John Wiley & Sons, Ltd., 1674.

Young, D. S. (1987), "Random Vectors and Spatial Analysis by Geostatistics for Geotechnical Applications," *Mathematical Geology,* 19(6), 467-479.

Zeileis, A., Hornik, K., and Murrell, P. (2008), "Escaping RGBland: Selecting Colors for Statistical Graphics," *Computational Statistics & Data Analysis*, a preprint of an article accepted for publication at URL http://statmath.wu-wien.ac.at/~zeileis/papers/Zeileis+Hornik+Murrell-2009.pdf.

Zippi, P. A. (2001), Vector Rose, URL http://www.pazsoftware.com/VectorRose.html.

APPENDICES

Appendix A

Notation

A nonbolded lower case letter indicates a scalar. For example, λ is the scalar Lagrange multiplier, θ_i is the i^{th} observed direction in radians, and θ_{ij} is the angle between the i^{th} and the j^{th} observed directions in radians.

A bolded lower case letter indicates a vector. For example, with superscript "T" indicating the transpose, $\boldsymbol{w} = [w_1 \quad w_2 \quad \cdots \quad w_n]^T$ is an n-component column vector containing real scalar weights w_i. $\boldsymbol{x}_i, i = 0,\ldots, n,$ are vectors of physical locations where direction is measured. Location will be used to determine the distance between measurement locations, which in turn, will be used to estimate the spatial correlation structure. $\boldsymbol{u}_i, i = 1,\ldots, n,$ are 2-component unit vectors of observed direction at location $\boldsymbol{x}_i$.

A bolded capital letter indicates a matrix.

$\boldsymbol{U} = [\boldsymbol{u}_1 \quad \boldsymbol{u}_2 \quad \cdots \quad \boldsymbol{u}_n] = \begin{bmatrix} \cos(\theta_1) & \cos(\theta_2) & \cdots & \cos(\theta_n) \\ \sin(\theta_1) & \sin(\theta_2) & \cdots & \sin(\theta_n) \end{bmatrix}$ is a sample as a matrix whose columns are directions as unit vectors. The first row is a vector of the horizontal components. The second row is a vector of the vertical components.

Equation numbers are denoted by (*m.n*) with *m* the chapter number or appendix letter, and *n* a sequential number.

Appendix B

Linear Algebra

B.1 Identities for Vectors

Let $\boldsymbol{u}_i$ and $\boldsymbol{u}_j$ be unit vectors in R^2 with directions θ_i and θ_j in radians, and θ_{ij} be the angle in radians between $\boldsymbol{u}_i$ and $\boldsymbol{u}_j$.

$$\cos(\theta_i - \theta_j) \overset{\text{Trig Identity}}{=} \cos(\theta_i)\cos(\theta_j) + \sin(\theta_i)\sin(\theta_j) \overset{\text{Unit Vectors}}{=}$$

$$u_{i1}u_{j1} + u_{i2}u_{j2} \overset{*}{=} \boldsymbol{u}_i^T\boldsymbol{u}_j \overset{\text{Unit Vectors}}{=} \frac{\boldsymbol{u}_i^T\boldsymbol{u}_j}{\|\boldsymbol{u}_i\|\|\boldsymbol{u}_j\|} \overset{**}{=} \cos(\theta_{ij}) \tag{B.1}$$

* (Edwards and Penney 1988, p. 211, eq. 1), ** (Edwards and Penney 1988, p. 142, eq. 6)

$$\|\boldsymbol{v}\| = \sqrt{\boldsymbol{v}^T\boldsymbol{v}} \tag{B.2}$$

B.2 Some Properties of the Positive Definite Matrix $\boldsymbol{K}$

- A matrix $\boldsymbol{K}$ is positive definite (P. D.) if and only if there exists an invertible matrix $\boldsymbol{P}$ such that $\boldsymbol{K} = \boldsymbol{P}\boldsymbol{P}^T$.
- $\boldsymbol{K}^T = \left(\boldsymbol{P}\boldsymbol{P}^T\right)^T = \boldsymbol{P}\boldsymbol{P}^T = \boldsymbol{K} \Rightarrow$ $\boldsymbol{K}$ symmetric.
- $\boldsymbol{c}^T\boldsymbol{K}\boldsymbol{c} = \boldsymbol{c}^T\boldsymbol{P}\boldsymbol{P}^T\boldsymbol{c} \equiv \boldsymbol{d}^T\boldsymbol{d} = \sum_i d_i^2 \overset{\boldsymbol{P}\text{ non-singular, }\boldsymbol{c}\neq\boldsymbol{0}}{>} 0 \Rightarrow \boldsymbol{K}\text{ P. D.} \Rightarrow \boldsymbol{c}^T\boldsymbol{K}\boldsymbol{c} > 0, \forall \boldsymbol{c} \neq \boldsymbol{0}$
- Let $\boldsymbol{Q}$ and $\boldsymbol{\Lambda}$ be the eigenvector and diagonal eigenvalue matrices of $\boldsymbol{K}$.

$$\begin{aligned} 0 &\overset{\forall \boldsymbol{x}\neq\boldsymbol{0}}{<} \boldsymbol{x}^T\boldsymbol{K}\boldsymbol{x} \\ &= \boldsymbol{x}^T\boldsymbol{Q}\boldsymbol{\Lambda}\boldsymbol{Q}^T\boldsymbol{x} \\ &\overset{\boldsymbol{y}=\boldsymbol{Q}^T\boldsymbol{x}}{=} \boldsymbol{y}^T\boldsymbol{\Lambda}\boldsymbol{y} \\ &\overset{\Lambda\text{ Diag}}{=} \sum_i y_i^2\lambda_i \end{aligned}$$

$$\overset{\text{Let } \boldsymbol{y}=\boldsymbol{e}_i,\ \text{elementary vector}}{\Rightarrow} \quad \lambda_i > 0 \Rightarrow$$

$$\boldsymbol{K}\ \text{P. D.} \Rightarrow \lambda_i \text{ of } \boldsymbol{\Lambda} > 0$$

Reversing the order of the proof, leads to

$$\lambda_i \text{ of } \boldsymbol{\Lambda} > 0 \Leftrightarrow \boldsymbol{K}\ \text{P. D.} \tag{B.3}$$

B.3 Theorem: The P. D. Matrix Has an Inverse

$$\begin{aligned}
\boldsymbol{K} &\overset{B.2}{=} \boldsymbol{P}\boldsymbol{P}^T \Rightarrow \\
\boldsymbol{K}^{-1} &= \left(\boldsymbol{P}\boldsymbol{P}^T\right)^{-1} \\
&\overset{\boldsymbol{P}\ \text{invertible}}{=} \left(\boldsymbol{P}^T\right)^{-1}\boldsymbol{P}^{-1}. \\
\boldsymbol{P}^T\left(\boldsymbol{P}^{-1}\right)^T &= \left(\boldsymbol{P}^{-1}\boldsymbol{P}\right)^T \\
&= \boldsymbol{I}^T \\
&= \boldsymbol{I} \Rightarrow \\
\left(\boldsymbol{P}^{-1}\right)^T &= \left(\boldsymbol{P}^T\right)^{-1} \Rightarrow \\
\boldsymbol{K}^{-1} &= \left(\boldsymbol{P}^T\right)^{-1}\boldsymbol{P}^{-1} \\
&= \left(\boldsymbol{P}^{-1}\right)^T\boldsymbol{P}^{-1} \Rightarrow
\end{aligned}$$

$$\boldsymbol{K}^{-1} = \left(\boldsymbol{P}^{-1}\right)^T\boldsymbol{P}^{-1} \tag{B.4}$$

B.4 Theorem: The Inverse of P. D. Matrix Is Symmetric

$$\begin{aligned}
\boldsymbol{K}^{-1}\boldsymbol{K} &= \boldsymbol{I} \\
&= \boldsymbol{I}^T \\
&= \left(\boldsymbol{K}\boldsymbol{K}^{-1}\right)^T \\
&= \left(\boldsymbol{K}^{-1}\right)^T\boldsymbol{K}^T \\
&\overset{\boldsymbol{K}=\boldsymbol{P}\boldsymbol{P}^T\ \text{symmetric}}{=} \left(\boldsymbol{K}^{-1}\right)^T\boldsymbol{K} \Rightarrow \\
\boldsymbol{K}^{-1}\boldsymbol{K}\boldsymbol{K}^{-1} &= \left(\boldsymbol{K}^{-1}\right)^T\boldsymbol{K}\boldsymbol{K}^{-1} \Rightarrow \\
\boldsymbol{K}^{-1} &= \left(\boldsymbol{K}^{-1}\right)^T \Rightarrow
\end{aligned}$$

$$\boldsymbol{K}^{-1} = \left(\boldsymbol{K}^{-1}\right)^T \tag{B.5}$$

B.5 Theorem: The Inverse of P. D. Matrix Is P. D.

$$
\begin{aligned}
\boldsymbol{K}^{-1} &= \left(\boldsymbol{P}\boldsymbol{P}^T\right)^{-1} \\
&= \left(\boldsymbol{P}^T\right)^{-1}\boldsymbol{P}^{-1} \\
&\overset{B.3:\left(\boldsymbol{P}^{-1}\right)^T=\left(\boldsymbol{P}^T\right)^{-1}}{=} \left(\boldsymbol{P}^{-1}\right)^T\boldsymbol{P}^{-1} \\
&\overset{\boldsymbol{Q}^T=\boldsymbol{P}^{-1}}{=} \boldsymbol{Q}\boldsymbol{Q}^T .
\end{aligned}
$$

$$\boldsymbol{Q}^T = \boldsymbol{P}^{-1} \Rightarrow \boldsymbol{Q} = \left(\boldsymbol{P}^{-1}\right)^T .$$

$$\boldsymbol{P}^T\left(\boldsymbol{P}^{-1}\right)^T = \left(\boldsymbol{P}^{-1}\boldsymbol{P}\right)^T = \boldsymbol{I} \Rightarrow$$

$$\boldsymbol{Q}\ \textit{invertible} \Rightarrow \boldsymbol{K}^{-1} = \boldsymbol{Q}\boldsymbol{Q}^T \text{ P. D.}$$

$$\boldsymbol{K}\text{ P.D.} \Rightarrow \boldsymbol{K}^{-1}\text{ P.D.} \tag{B.6}$$

B.6 Some Properties of the Negative Definite Matrix

- A matrix $\boldsymbol{K}$ is negative definite (N. D.) if $\boldsymbol{c}^T\boldsymbol{K}\boldsymbol{c} < 0\ \forall \boldsymbol{c} \neq \boldsymbol{0}$.
- $\boldsymbol{K}$ N. D. $\Rightarrow -\boldsymbol{K} \equiv \boldsymbol{M}$ P. D. $\Rightarrow \boldsymbol{K}^T = \left(-\boldsymbol{M}\right)^T = -\boldsymbol{M} = \boldsymbol{K} \Rightarrow \boldsymbol{K}$ symmetric.
- This Th. will prove that the eigenvalues of a N. D. matrix are negative. Let $\boldsymbol{Q}$ and $\boldsymbol{\Lambda}$ be the eigenvector and diagonal eigenvalue matrices of $\boldsymbol{K}$, respectively.

$\boldsymbol{K}$ *N. D.* $\Rightarrow$

$$
\begin{aligned}
0 &\overset{\forall \boldsymbol{x}\neq\boldsymbol{0}}{>} \boldsymbol{x}^T\boldsymbol{K}\boldsymbol{x} \\
&= \boldsymbol{x}^T\boldsymbol{Q}\boldsymbol{\Lambda}\boldsymbol{Q}^T\boldsymbol{x} \\
&\overset{\boldsymbol{y}=\boldsymbol{Q}^T\boldsymbol{x}}{=} \boldsymbol{y}^T\boldsymbol{\Lambda}\boldsymbol{y} \\
&= \sum_i y_i^2\lambda_i \\
&\overset{\text{Let } \boldsymbol{y}=\boldsymbol{e}_j,\ \textit{elementary vector}}{\Rightarrow} \quad 0 > \lambda_i \Rightarrow
\end{aligned}
$$

$$\boldsymbol{K}\text{ N. D.} \Rightarrow \lambda_i \text{ of } \boldsymbol{\Lambda} < 0$$

Reversing the order of the proof, leads to

$$\lambda_i \text{ of } \boldsymbol{\Lambda} < 0 \Leftrightarrow \boldsymbol{K} \text{ N. D.} \tag{B.7}$$

B.7 Derivatives Required for Kriging

Let $\boldsymbol{c} = \begin{bmatrix} c_1 & \cdots & c_n \end{bmatrix}^T$ and $\boldsymbol{w} = \begin{bmatrix} w_1 & \cdots & w_n \end{bmatrix}^T \Rightarrow \boldsymbol{w}^T\boldsymbol{c} = w_1c_1 + \cdots + w_nc_n$.

$$\frac{\partial}{\partial \boldsymbol{w}}\left(\boldsymbol{w}^T\boldsymbol{c}\right) \equiv \begin{bmatrix} \frac{\partial}{\partial w_1}\left(\boldsymbol{w}^T\boldsymbol{c}\right) \\ \frac{\partial}{\partial w_2}\left(\boldsymbol{w}^T\boldsymbol{c}\right) \\ \vdots \\ \frac{\partial}{\partial w_n}\left(\boldsymbol{w}^T\boldsymbol{c}\right) \end{bmatrix}$$

$$= \begin{bmatrix} \frac{\partial}{\partial w_1}\left(w_1c_1 + \cdots + w_nc_n\right) \\ \vdots \\ \frac{\partial}{\partial w_n}\left(w_1c_1 + \cdots + w_nc_n\right) \end{bmatrix}$$

$$= \begin{bmatrix} c_1 \\ \vdots \\ c_n \end{bmatrix} = \boldsymbol{c} \Rightarrow$$

$$\frac{\partial}{\partial \boldsymbol{w}}\left(\boldsymbol{w}^T\boldsymbol{c}\right) = \boldsymbol{c} \tag{B.8}$$

Let $\boldsymbol{K} = \begin{bmatrix} k_{11} & \cdots & k_{1n} \\ \vdots & \ddots & \vdots \\ k_{1n} & \cdots & k_{nn} \end{bmatrix}$ be symmetric and

$$\boldsymbol{w}^T\boldsymbol{K}\boldsymbol{w} = k_{11}w_1^2 + 2k_{12}w_1w_2 + \cdots + 2k_{1n}w_1w_n + \cdots + k_{nn}w_n^2 \Rightarrow$$

$$\frac{\partial}{\partial \boldsymbol{w}}\left(\boldsymbol{w}^T\boldsymbol{K}\boldsymbol{w}\right) \equiv \begin{bmatrix} \frac{\partial}{\partial w_1}\left(\boldsymbol{w}^T\boldsymbol{K}\boldsymbol{w}\right) \\ \vdots \\ \frac{\partial}{\partial w_n}\left(\boldsymbol{w}^T\boldsymbol{K}\boldsymbol{w}\right) \end{bmatrix}$$

$$= \begin{bmatrix} 2k_{11}w_1 + \cdots + 2k_{1n}w_n \\ \vdots \\ 2k_{1n}w_1 + \cdots + 2k_{nn}w_n \end{bmatrix}$$

$$= 2\begin{bmatrix} k_{11} & \cdots & k_{1n} \\ \vdots & \ddots & \vdots \\ k_{1n} & \cdots & k_{nn} \end{bmatrix}\begin{bmatrix} w_1 \\ \vdots \\ w_n \end{bmatrix}$$
$$= 2\boldsymbol{K}\boldsymbol{w} \Rightarrow$$

$$\frac{\partial}{\partial \boldsymbol{w}}\left(\boldsymbol{w}^T \boldsymbol{K}\boldsymbol{w}\right) = 2\boldsymbol{K}\boldsymbol{w} \tag{B.9}$$

The following derivative is required by (B.11). Let $\boldsymbol{y} = \boldsymbol{K}\boldsymbol{w} \Rightarrow y_i = \sum_j K_{ij} w_j$.

$$\frac{\partial \boldsymbol{K}\boldsymbol{w}}{\partial \boldsymbol{w}} = \left(\frac{\partial}{\partial \boldsymbol{w}}\right)\boldsymbol{y}^T$$
$$= \begin{pmatrix} \frac{\partial}{\partial w_1} \\ \vdots \\ \frac{\partial}{\partial w_n} \end{pmatrix}\begin{pmatrix} y_1 & \cdots & y_n \end{pmatrix}$$
$$= \begin{pmatrix} \frac{\partial y_1}{\partial w_1} & \cdots & \frac{\partial y_n}{\partial w_1} \\ \vdots & & \vdots \\ \frac{\partial y_1}{\partial w_n} & \cdots & \frac{\partial y_n}{\partial w_n} \end{pmatrix}$$
$$= \begin{pmatrix} K_{11} & \cdots & K_{n1} \\ \vdots & & \vdots \\ K_{1n} & \cdots & K_{nn} \end{pmatrix}$$

$$\overset{B.2}{=} \begin{pmatrix} K_{11} & \cdots & K_{1n} \\ \vdots & & \vdots \\ K_{n1} & \cdots & K_{nn} \end{pmatrix}$$

$$= \boldsymbol{K} \Rightarrow$$

$$\frac{\partial \boldsymbol{K}\boldsymbol{w}}{\partial \boldsymbol{w}} = \boldsymbol{K} \tag{B.10}$$

B.8 The Requirements for Maximization

Theorems 1.51 and 1.52 (a) from Rencher (1975) are required to show that the kriging solution is a maximum.

B.8.1 Theorem 1.51

"If $u = f(w_1, w_2, \ldots, w_n)$ is such that all the first and second partial derivatives are continuous, and if $\boldsymbol{B}$ is the matrix whose $(i, j)^{th}$ element is $\frac{\partial^2 u}{\partial w_i \partial w_j}$, then at the point where $\frac{\partial u}{\partial \boldsymbol{w}} = \boldsymbol{0}$, u has a minimum if $\boldsymbol{B}$ is positive definite and a maximum if $\boldsymbol{B}$ is negative definite." In one-dimensional calculus, the first derivative of a function is decreasing where the second derivative is negative. Hence, at the point where the first derivative is zero and the second derivative is negative, the function is at a maximum. In multi-dimensional calculus, the corresponding second derivative is a matrix of second partial derivatives called the Hessian. Where the first derivatives are zero and the Hessian is negative definite, the function is at a maximum.

B.8.2 Theorem 1.52

"If $u = f(w_1, w_2, \ldots, w_n) = \boldsymbol{w}^T \boldsymbol{K} \boldsymbol{w} + \boldsymbol{w}^T \boldsymbol{c} + d$, where $\boldsymbol{K}$ is positive definite and d is a scalar, then the matrix $\boldsymbol{B} = \left(\frac{\partial^2 u}{\partial w_i \partial w_j} \right) = 2\boldsymbol{K}$."

$$\left(\frac{\partial^2 u}{\partial w_i \partial w_j}\right) = \left(\frac{\partial}{\partial w_j}\frac{\partial u}{\partial w_i}\right)$$

$$= \left(\frac{\partial}{\partial w_j}\frac{\partial\left(\boldsymbol{w}^T\boldsymbol{K}\,\boldsymbol{w} + \boldsymbol{w}^T\boldsymbol{c} + d\right)}{\partial w_i}\right)$$

$$\overset{(B.8),(B.9)}{=} \left(\frac{\partial\left(2\boldsymbol{K}\,\boldsymbol{w} + \boldsymbol{c}\right)}{\partial w_j}\right)$$

$$= \frac{\partial\left(2\boldsymbol{K}\,\boldsymbol{w} + \boldsymbol{c}\right)}{\partial \boldsymbol{w}}$$

$$= 2\frac{\partial\left(\boldsymbol{K}\,\boldsymbol{w}\right)}{\partial \boldsymbol{w}}$$

$$\overset{(B.10)}{=} 2\boldsymbol{K} \Rightarrow$$

$$\left(\frac{\partial^2 u}{\partial w_i \partial w_j}\right) = 2\boldsymbol{K} \tag{B.11}$$

B.9 Expectation

With $\boldsymbol{Z}$ a random matrix of elements Z_{ij}, or $\boldsymbol{Z} = [(Z_{ij})]$, and E the expectation operator, Seber (1977, p. 8) defined the expectation of a matrix as

$$\mathrm{E}\{\boldsymbol{Z}\} = \mathrm{E}\{[(Z_{ij})]\} = [(\mathrm{E}\{Z_{ij}\})] \tag{B.12}$$

Appendix C

Qualitative Evaluations of Other CRFs with Standardization

Appendix C extends the example of Chapter 5, Section 5.5, Figure 5-9, to other circular distributions: cardioid, triangular, uniform, and wrapped Cauchy. The purpose of these figures is to show that the method produces the desired distributional and spatial properties of the CRF. Figures C-1 to C-4 show the distributional fits on the left as QQ plots and the spatial properties of the samples on the right. Details of the interpretation are given in Chapter 5, Subsection 5.5.3. These figures were constructed as described in Chapter 5, Subsection 5.5.2 using the R code in Appendix L, Section L.8. To facilitate verification of the desired spatial properties, the spherical covariance model was chosen for the gaussian random field (GRF). With the spherical covariance, the sill (the plateau formed by the mean cosine at distances where the CRV are uncorrelated) and the range (the distance at which the mean cosine forms the sill) are easily recognized. The realizations of the GRF were standardized according to Chapter 5, Section 5.3, step 1) (Subsections 5.4.3 and 5.4.4). The mean resultant length parameter ρ was set to ½ of the maximum, which depends on the distribution (Table 5-1).

Generally, the resulting QQ plots were highly linear, indicating a high degree of fit. The spatial properties of the cosineogram on the bottom right are a mirror of the variogram, approximately. When sampling variation resulted in a GRF realization with less than ideal spatial properties, these properties were mirrored from the variogram plot of linear-spatial properties of the GRF to the cosineogram plot of the circular-spatial properties of the CRF. An assessment of each figure is given in the figure caption.

The examples in Appendix C were selected for close fit to the desired distribution and spatial properties. In Appendix D, the circular distribution parameters were set to

extremes, the figures were generated sequentially with random seeds, both nonstandardized and standardized results were computed, and the distributional and spatial properties were scored.

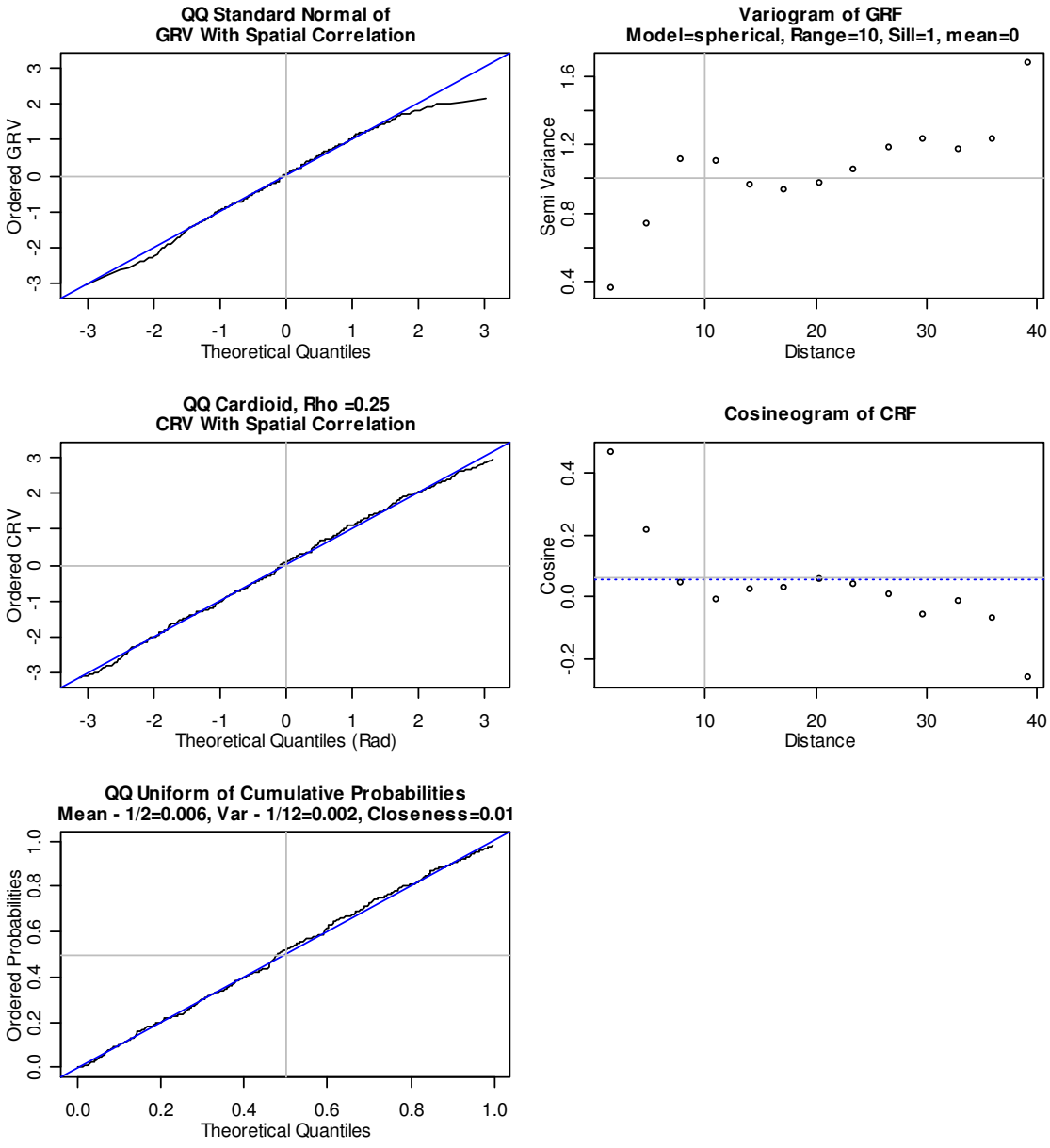

Figure C-1. Evaluation of a Cardioid CRF, $\rho = 0.25$, Overfit, Range $r = 10$. The linearity of the QQ plots indicates that the distributional fits are close. The spatial plots on the right show agreement with the desired spatial properties (range $r = 10$, sill $\approx \rho^2$).

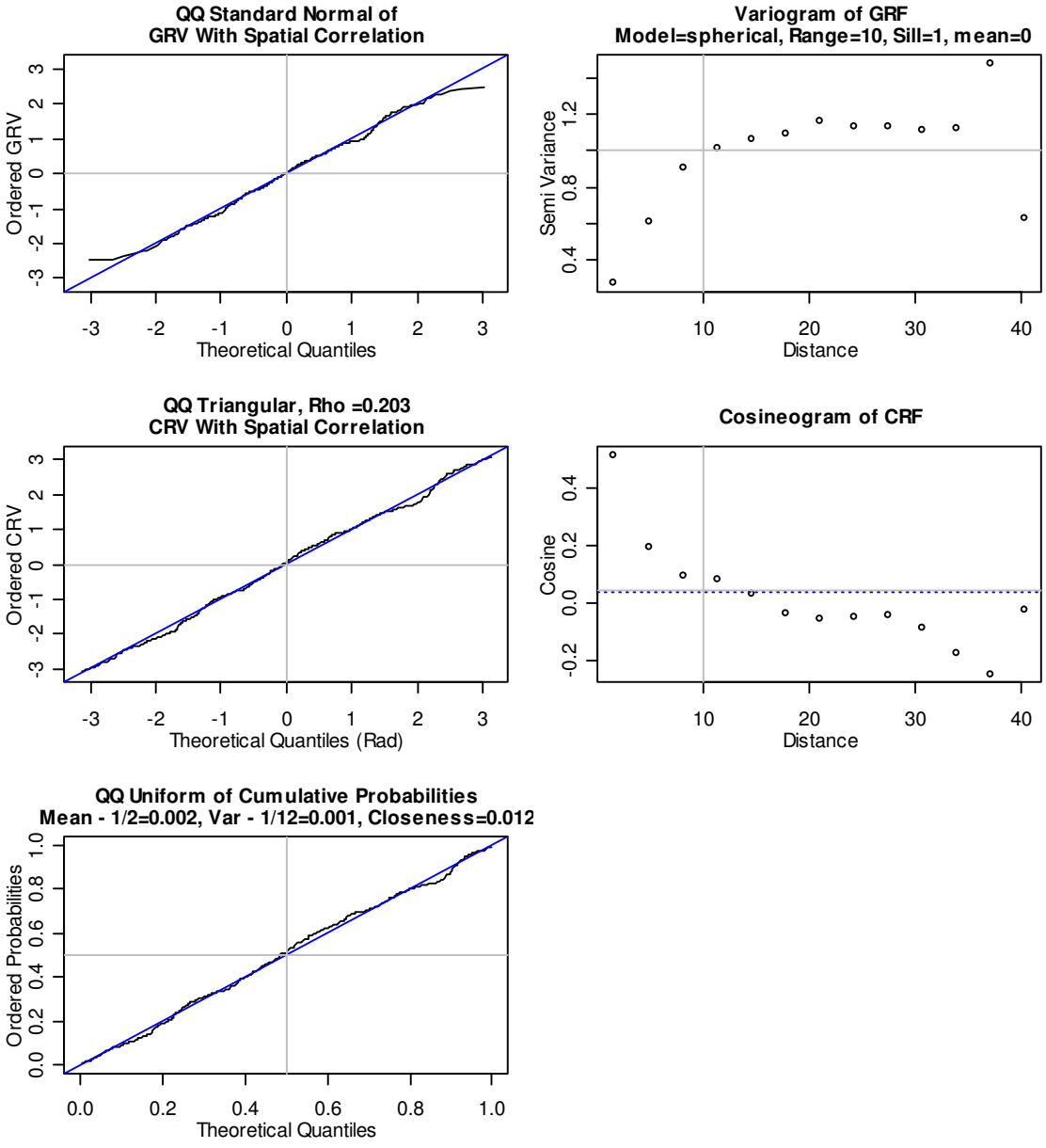

Figure C-2. Evaluation of a Triangular CRF, $\rho = 0.203$, Overfit, Range $r = 10$. The linearity of the QQ plots indicates that the distributional fits are close. The sill is not well defined in the spatial plots on the right. The range is between 10 and 20.

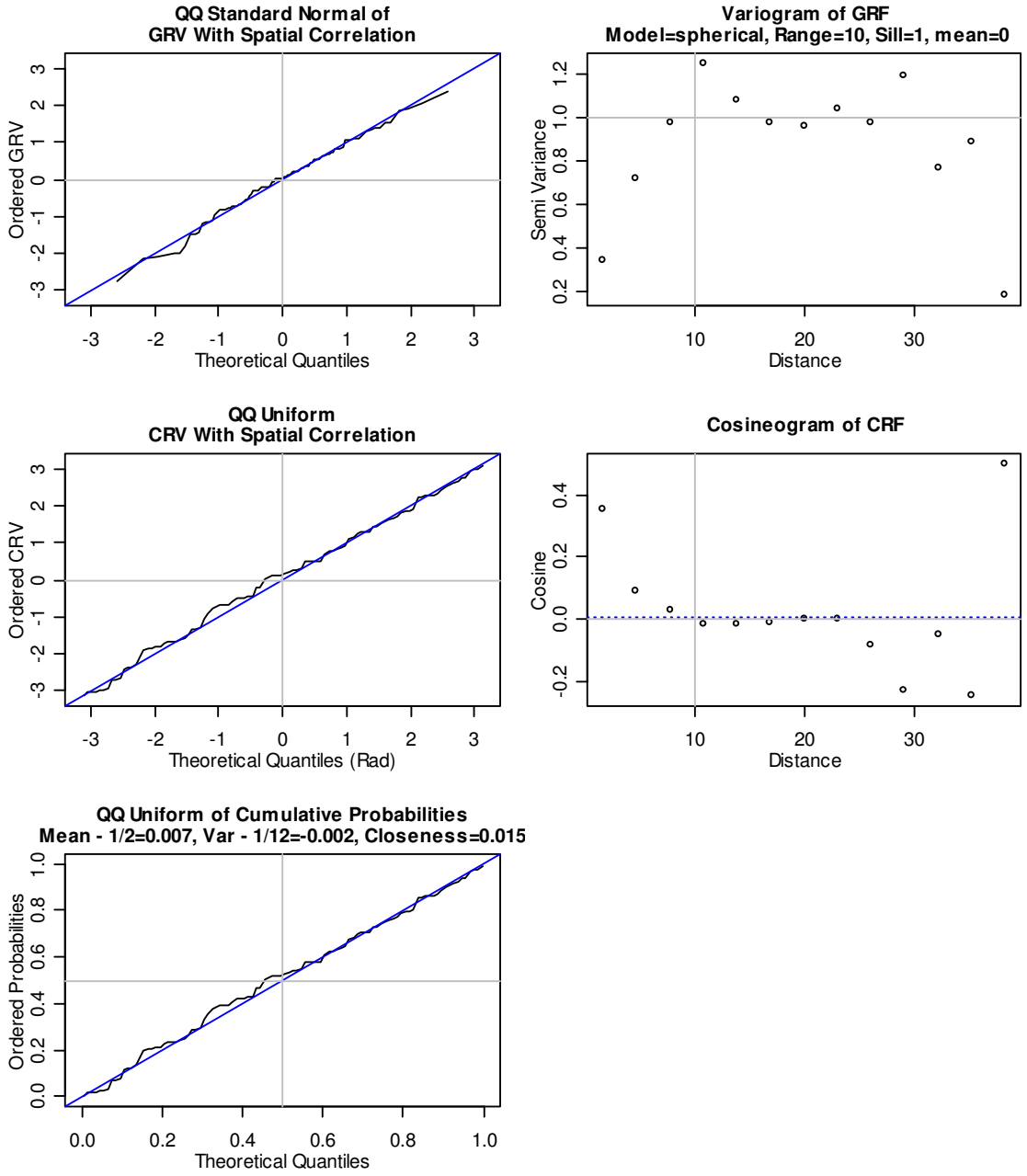

Figure C-3. Evaluation of a Uniform CRF, Overfit, Range $r = 10$. The linearity of the QQ plots indicates that the distributional fits are close. The spatial plots on the right show agreement with the desired spatial properties (range $r = 10$, sill=0).

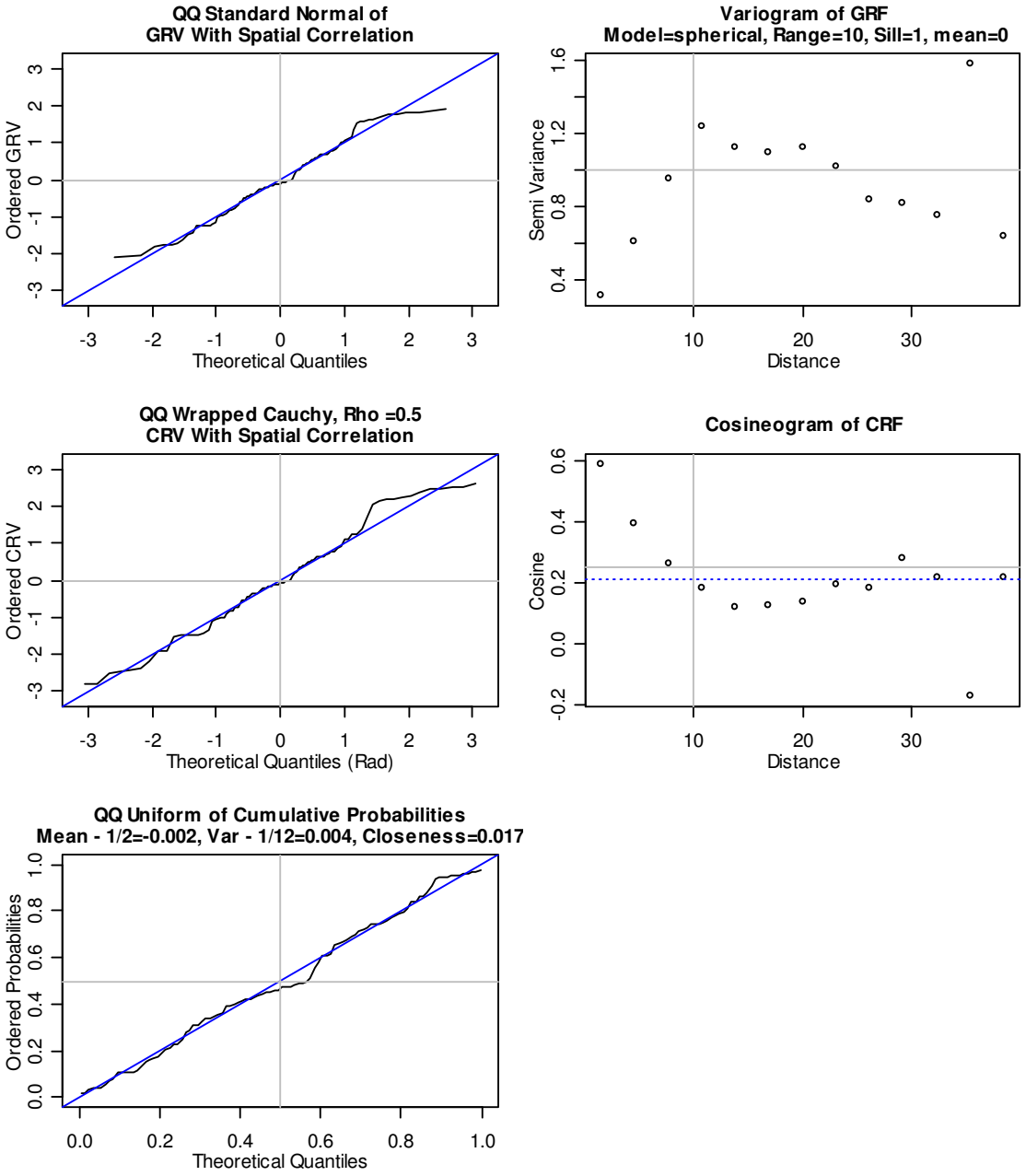

Figure C-4. Evaluation of a Wrapped Cauchy CRF, $\rho = 0.5$, Overfit, Range $r = 10$. The linearity of the QQ plots indicates that the distributional fits are close. The sill is not well defined in the spatial plots on the right. The sill of the variogram is high and the sill of the cosineogram is low. The range is between 10 and 15.

Appendix D

Qualitative Evaluations of CRFs Near Parameter Extremes

Appendix D extends the examples of Chapter 5, Section 5.5, Figure 5-8, and Appendix C to the selected circular distributions with mean resultant length parameter ρ at extremes of 0.05 and 95% of the maximum (Table 5-1). The purpose of these figures is to show that the method produces the desired distributional and spatial properties of the CRF. Standardized and nonstandardized realizations of the GRF with the same parameters were computed using the same random seed. Figures D-1 to D-16 show the distributional fits on the left as QQ plots and the spatial properties of the samples on the right. The interpretation is given in Chapter Subsection 5.5.3. These figures were constructed as described in Subsection 5.5.2 using the R code in Appendix L, Section L.8. To facilitate verification of the desired spatial properties, the spherical covariance model was chosen for the gaussian random field (GRF) because the spatial properties are easily recognized.

Generally, the QQ plots with standardization were highly linear, indicating a high degree of fit, but the QQ plots based on nonstandardized realizations showed typical sampling variation. The QQ wrapped Cauchy plot at high ρ showed a significant lack of distribution fit regardless of standardization. An assessment of each figure is given in the figure caption.

The cosineogram plot of circular-spatial properties mirrored the variogram plot of linear-spatial properties. When sampling variation resulted in a realization of the GRF with less than ideal spatial properties, these properties were mirrored in the cosineogram plot of the circular-spatial properties. The spatial assessments in the figure captions are summarized at the end of Appendix D. Standardization of the GRF had no apparent

effect on agreement of the spatial properties of a simulation with the desired spatial properties.

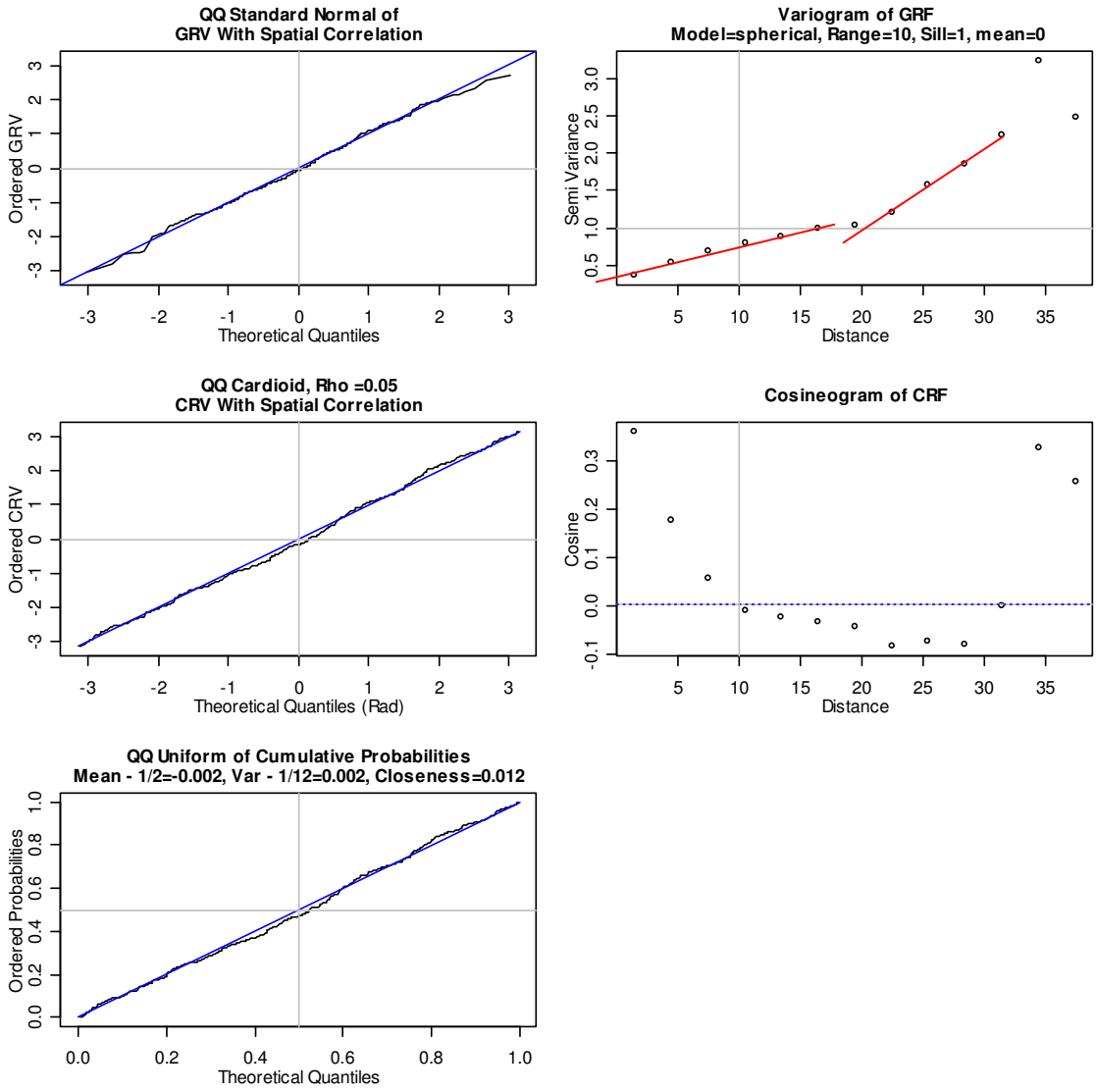

Figure D-1. Evaluation of a Cardioid CRF, $\rho = 0.05$, Overfit, Range $r = 10$. The linearity of the QQ plots indicates that the distributional fits are close. The sill is not well defined in the spatial plots on the right. The sill of the cosineogram is 0. Hence, the range is about 10.

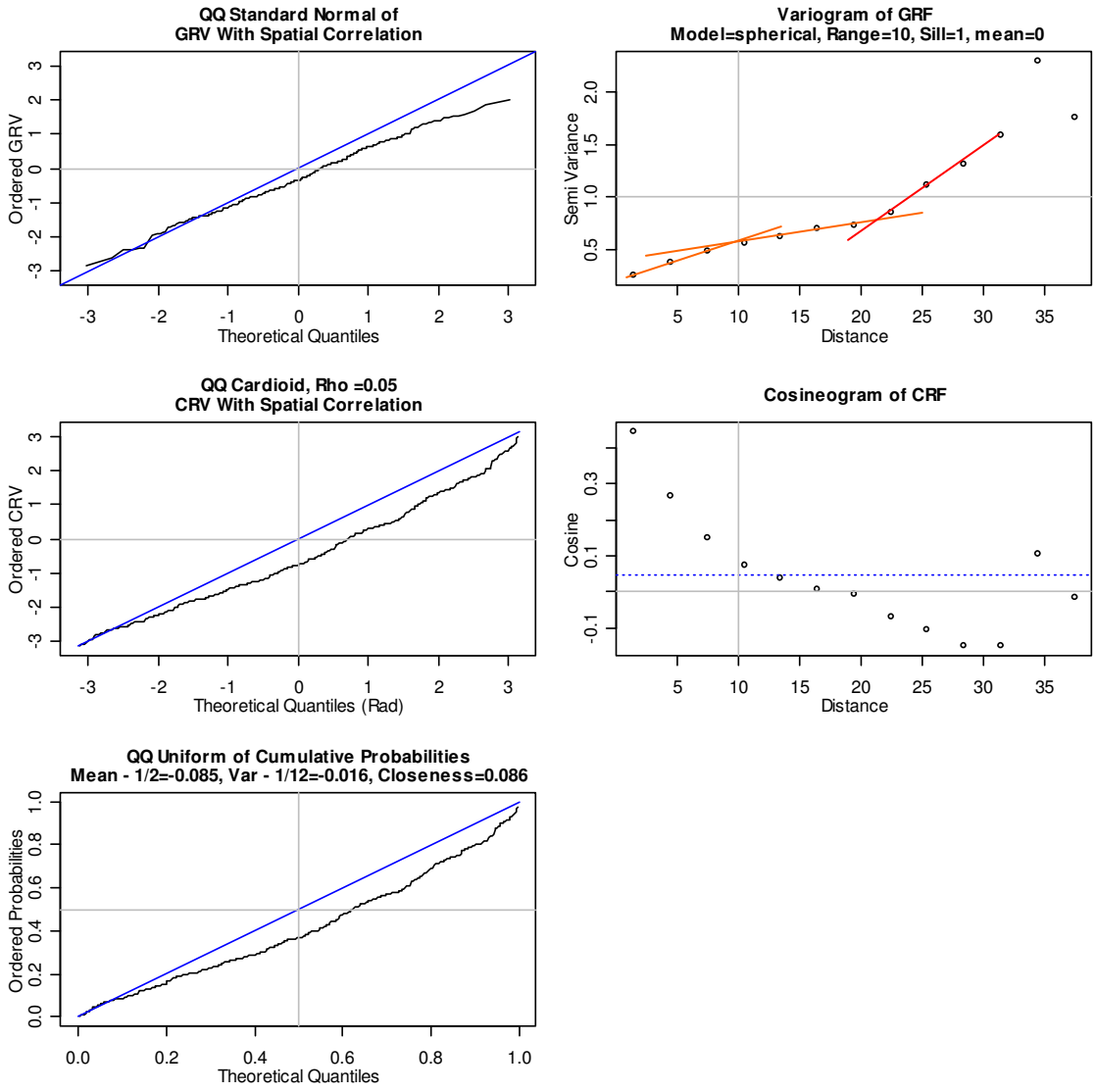

Figure D-2. Evaluation of a Cardioid CRF, $\rho = 0.05$, Range $r = 10$. The lack of linearity of the QQ plots is due to typical sampling variation. The sill is not well defined in the spatial plots on the right. The middle red line in the variogram may be the sill. Then, the range is about 10.

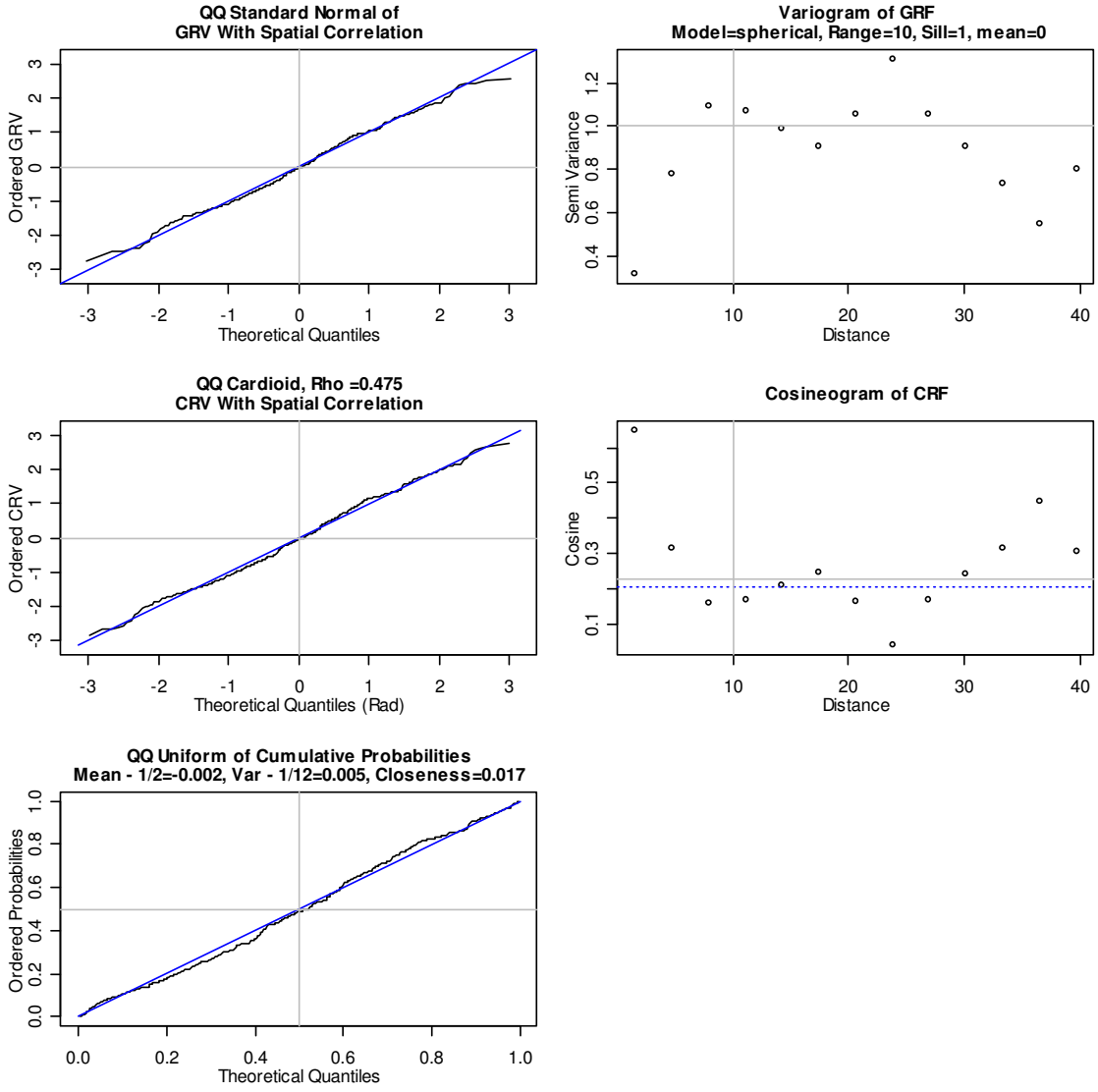

Figure D-3. Evaluation of a Cardioid CRF, $\rho = 0.475$, Overfit, Range $r = 10$. The linearity of the QQ plots indicates that the distributional fits are close. The spatial plots on the right indicate that the range is around 10 and the sill of the cosineogram is $\approx \rho^2$.

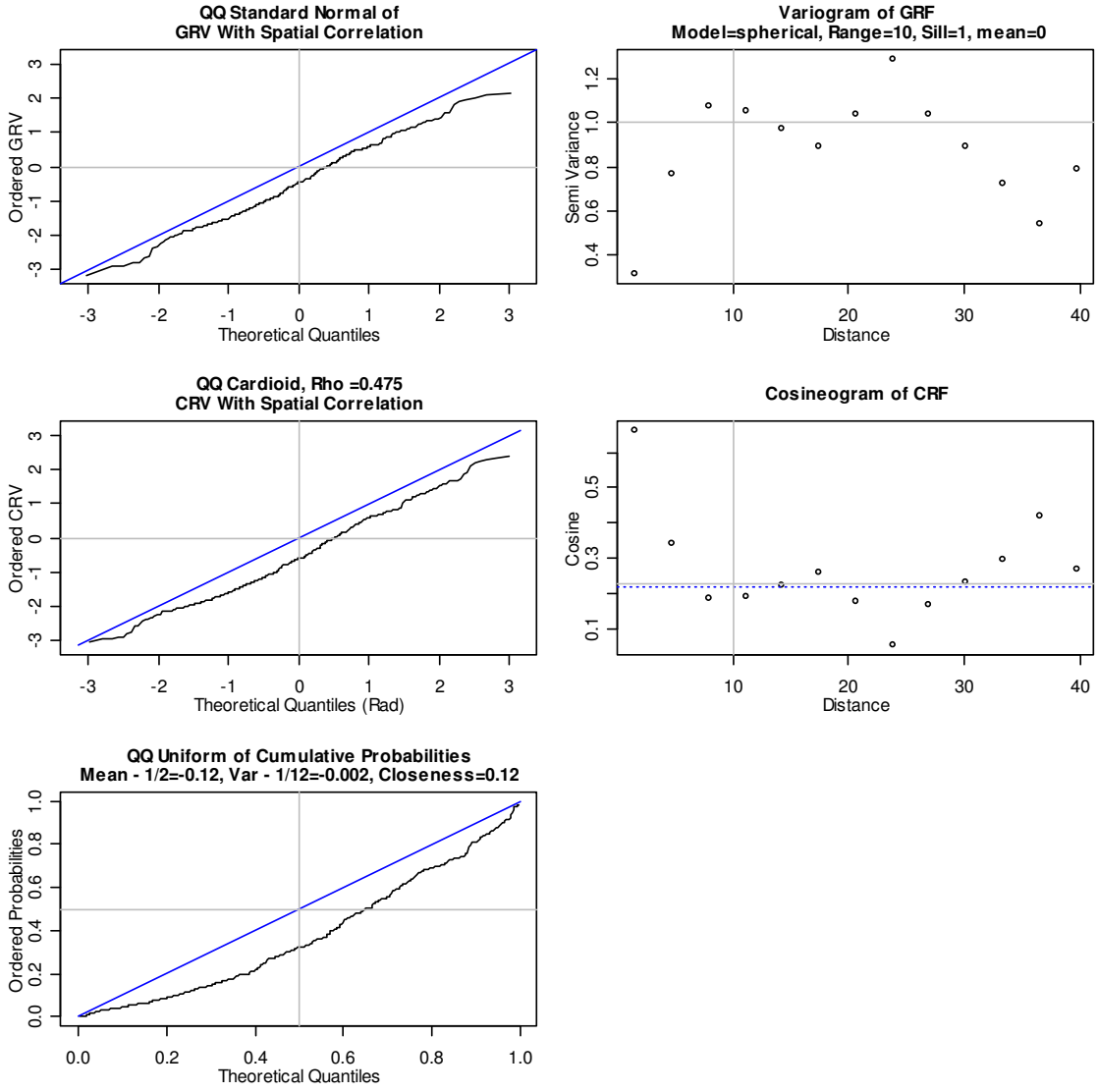

Figure D-4. Evaluation of a Cardioid CRF, $\rho = 0.475$, Range $r = 10$. The lack of linearity of the QQ plots is due to typical sampling variation. The spatial plots on the right indicate that the range is around 10 and the sill of the cosineogram is about ρ^2.

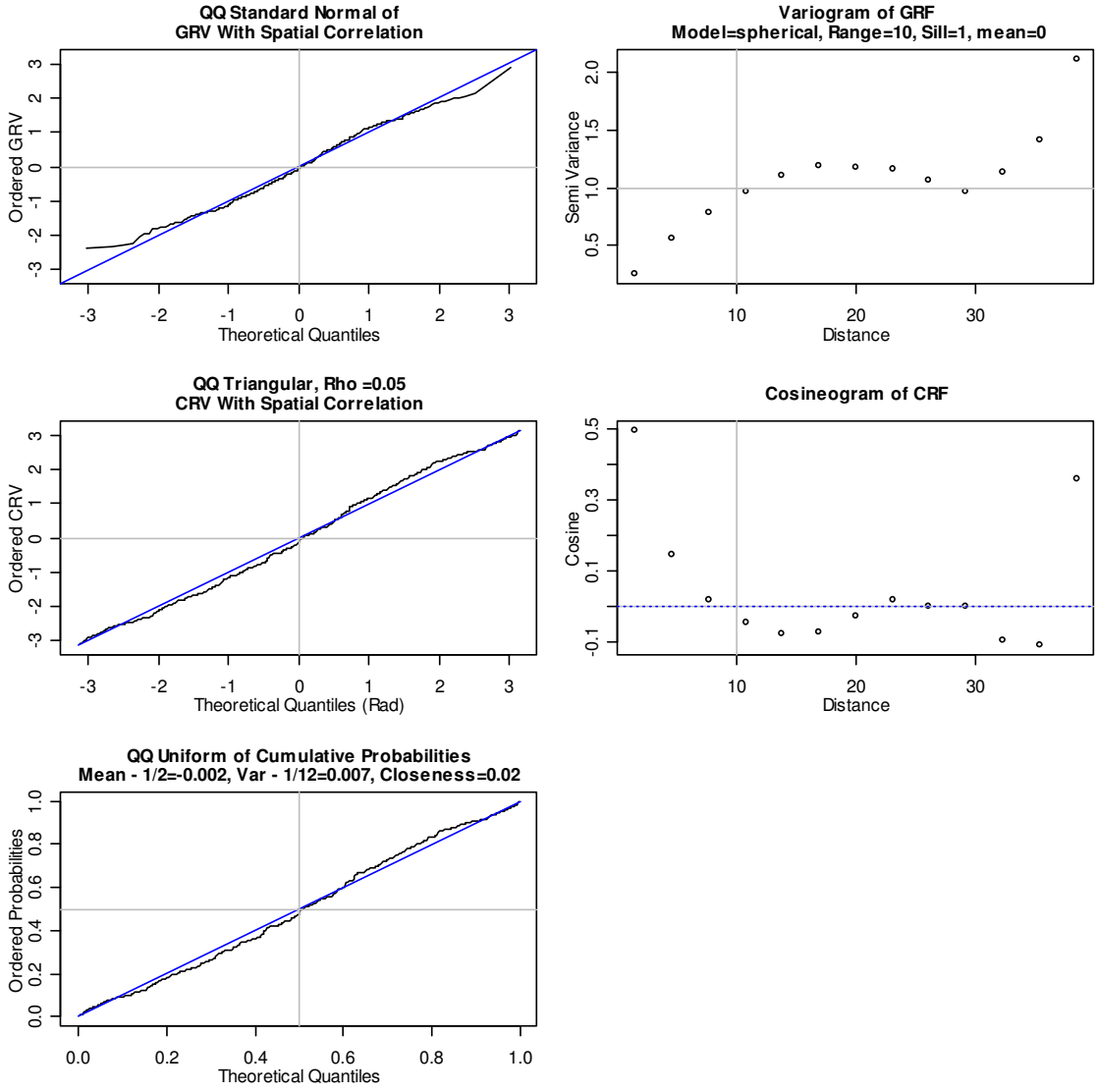

Figure D-5. Evaluation of a Triangular CRF, $\rho = 0.05$, Overfit, Range $r = 10$. The linearity of the QQ plots indicates that the distributional fits are close. The spatial plots on the right indicate that the range is about 10 and the sill of the cosineogram is 0.

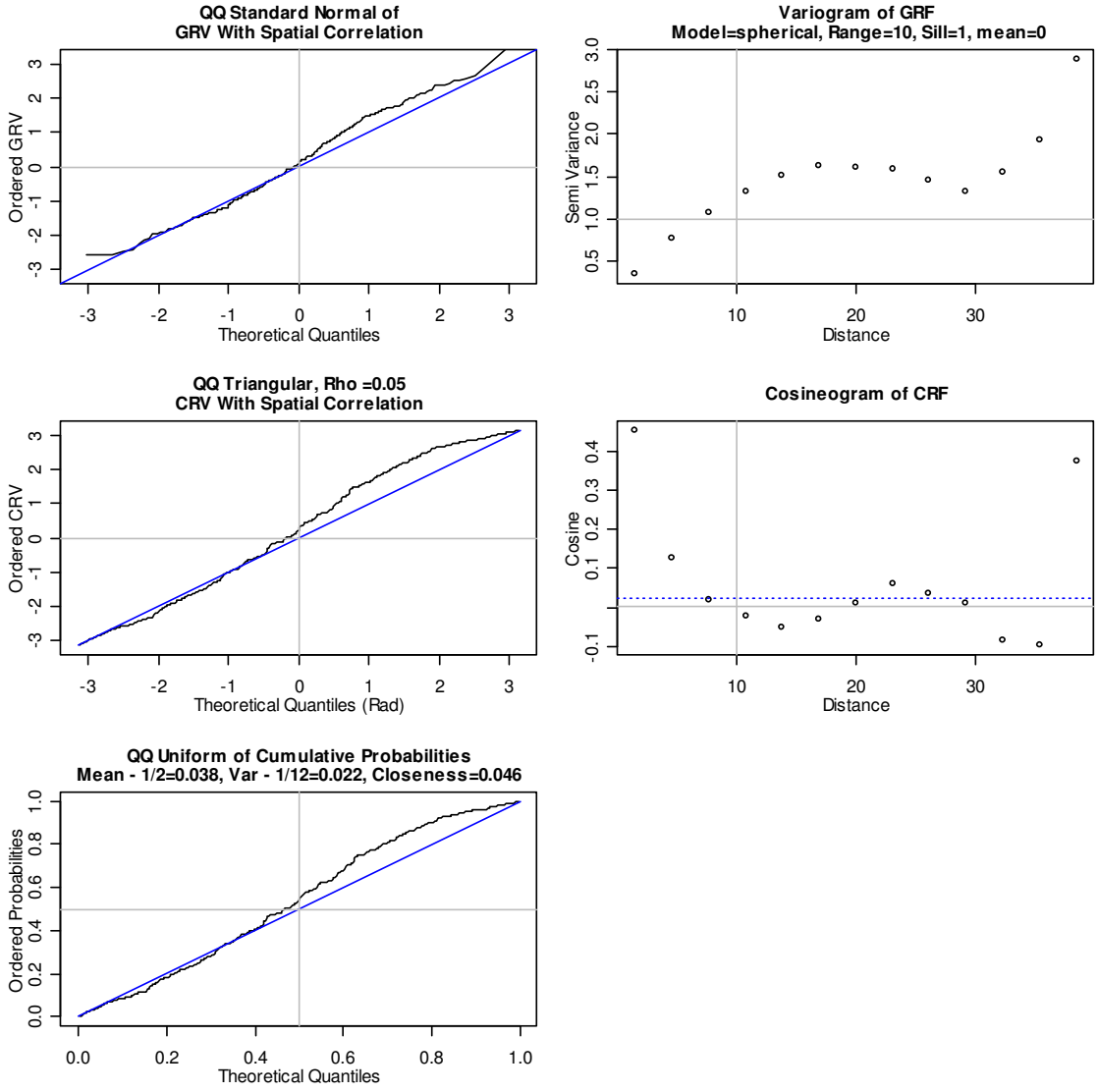

Figure D-6. Evaluation of a Triangular CRF, $\rho = 0.05$, Range $r = 10$. The lack of linearity of the QQ plots is due to typical sampling variation. The spatial plots on the right indicate that the range is around 10 and the sill is about 0.

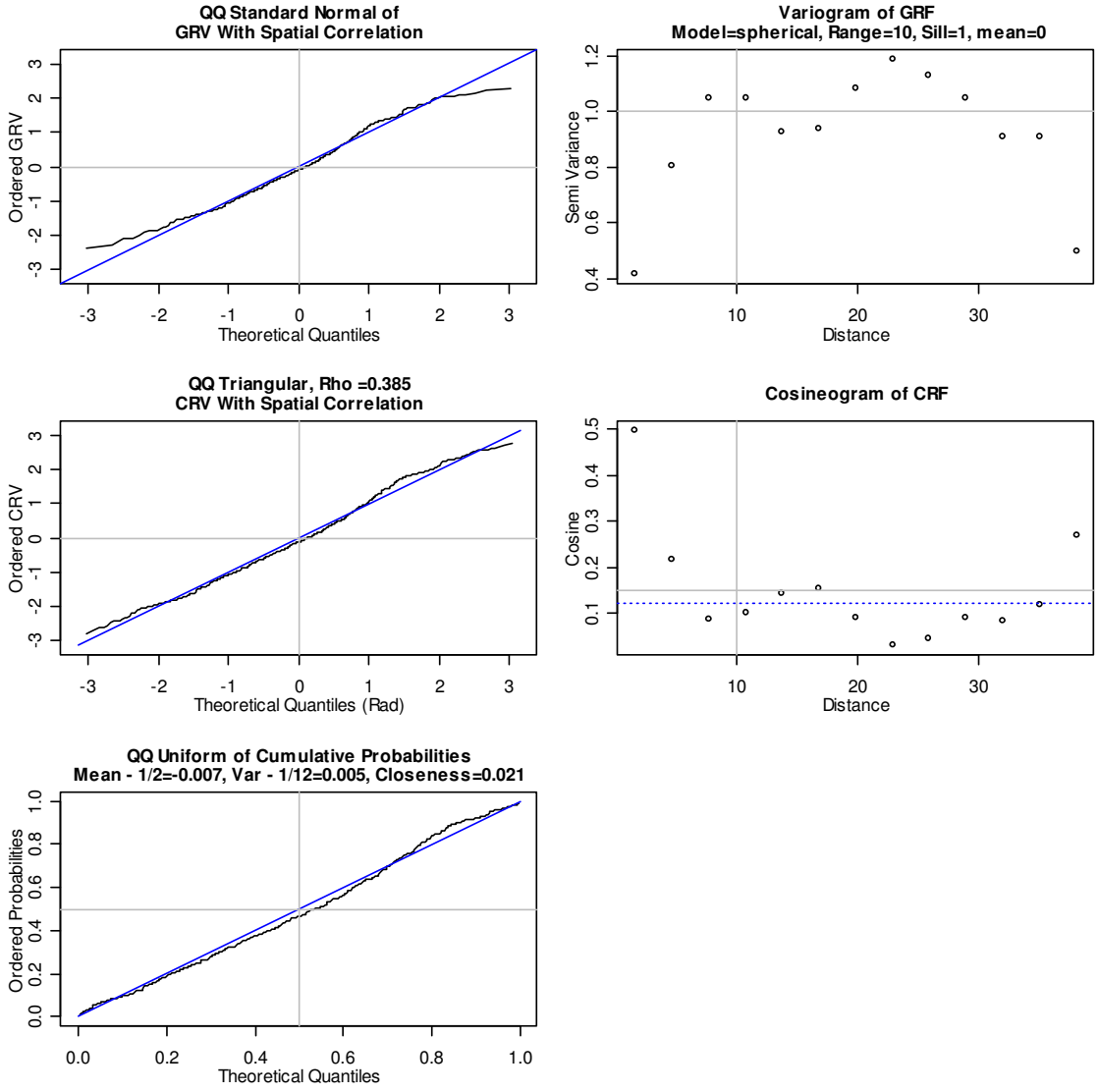

Figure D-7. Evaluation of a Triangular CRF, $\rho = 0.385$, Overfit, Range $r = 10$. The linearity of the QQ plots indicates that the distributional fits are close. The right plots indicate a range is about 10 and a sill of about $0.12 \approx \rho^2$.

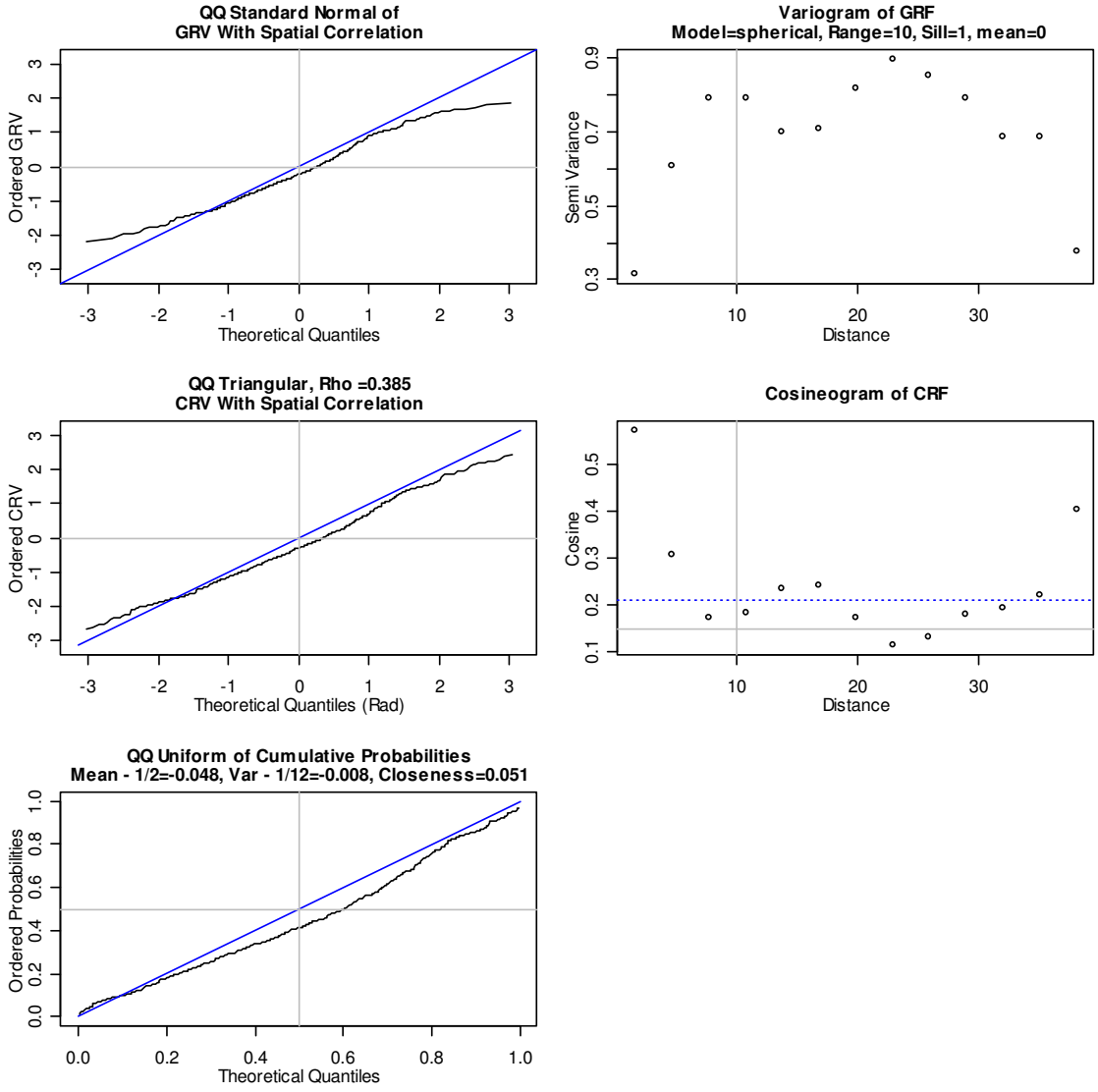

Figure D-8. Evaluation of a Triangular CRF, $\rho = 0.385$, Range $r = 10$. The lack of linearity of the QQ plots is due to typical sampling variation. The spatial plots on the right indicate that the range is about 10 and the sill is about 0.2 .

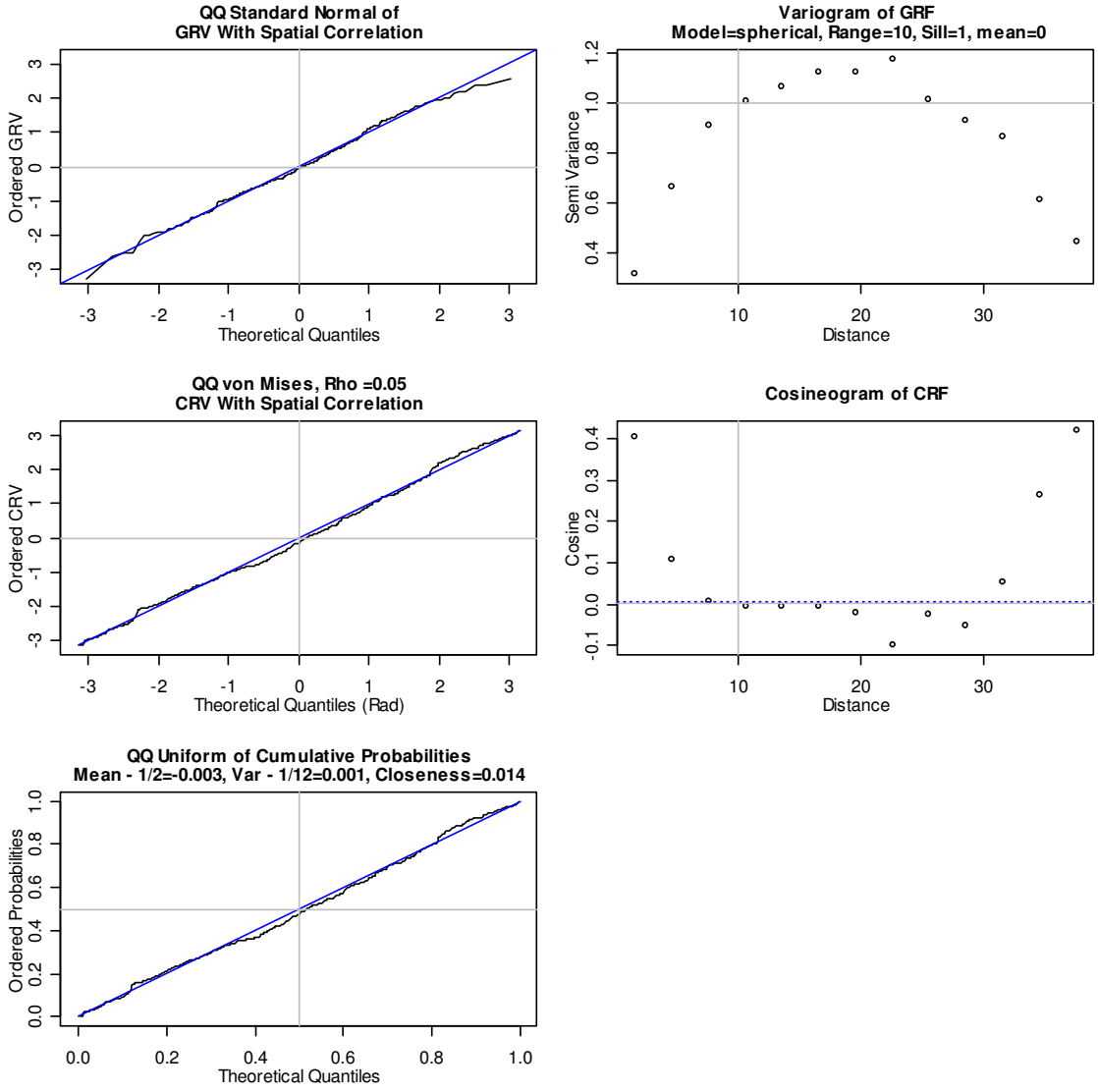

Figure D-9. Evaluation of a von Mises CRF, $\rho = 0.05$, Overfit, Range $r = 10$. The linearity of the QQ plots indicates that the distributional fits are close. The cosineogram plot shows agreement with the desired spatial characteristics (range $r = 10$, sill $\approx \rho^2$).

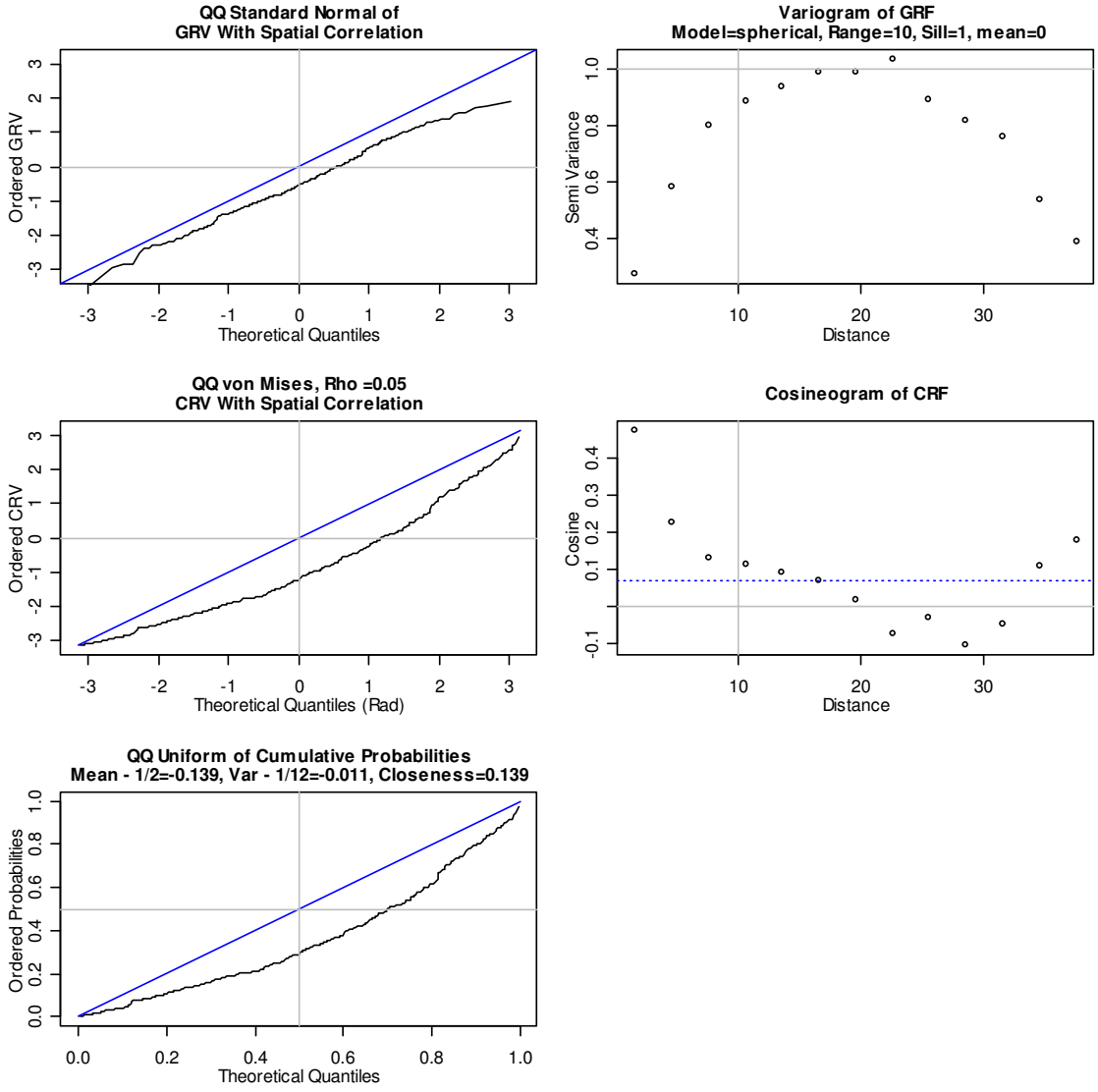

Figure D-10. Evaluation of a von Mises CRF, $\rho = 0.05$, Range $r = 10$. The lack of linearity of the QQ plots is due to typical sampling variation. The sill is not well defined in the right plots. The variogram suggest that the range is around 15.

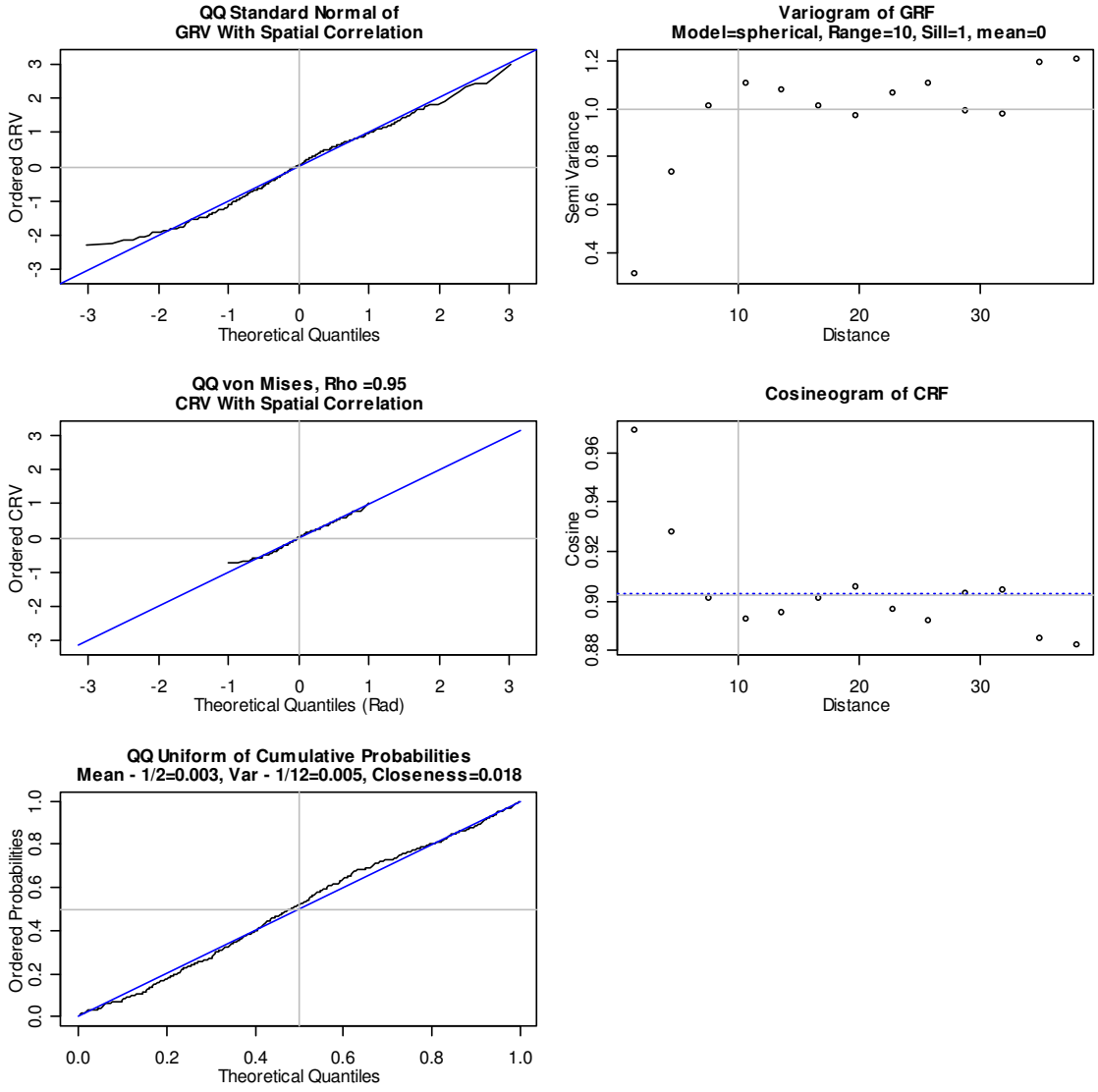

Figure D-11. Evaluation of a von Mises CRF, $\rho = 0.95$, Overfit, Range $r = 10$. The linearity of the QQ plots indicates that the distributional fits are close. The spatial plots on the right show agreement with the desired spatial characteristics (range $r = 10$, sill $\approx \rho^2$).

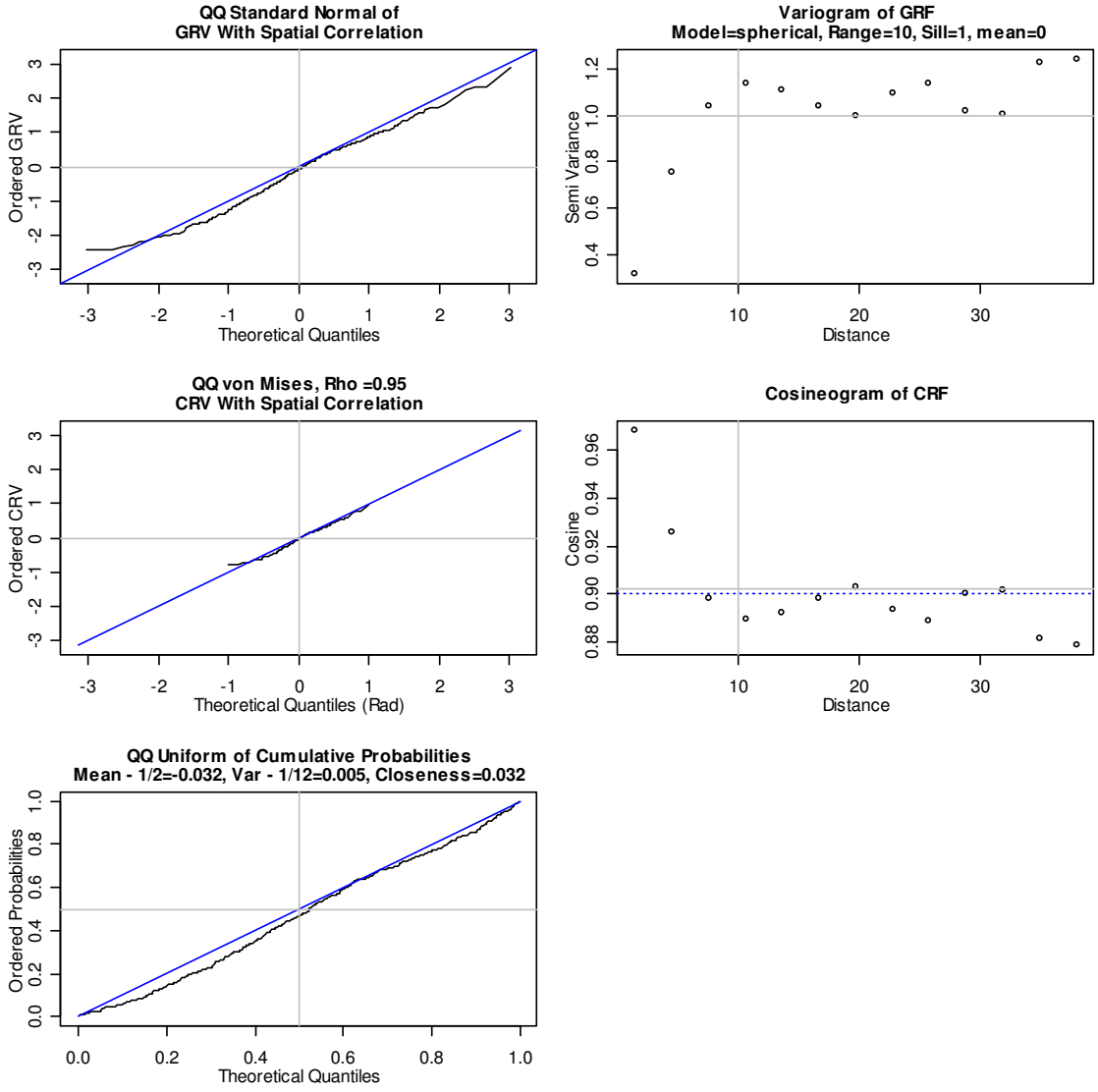

Figure D-12. Evaluation of a von Mises CRF, $\rho = 0.95$, Range $r = 10$. The lack of linearity of the QQ plots is due to typical sampling variation. The spatial plots on the right show agreement with the desired spatial characteristics (range r =10, sill= $0.90 \approx \rho^2$).

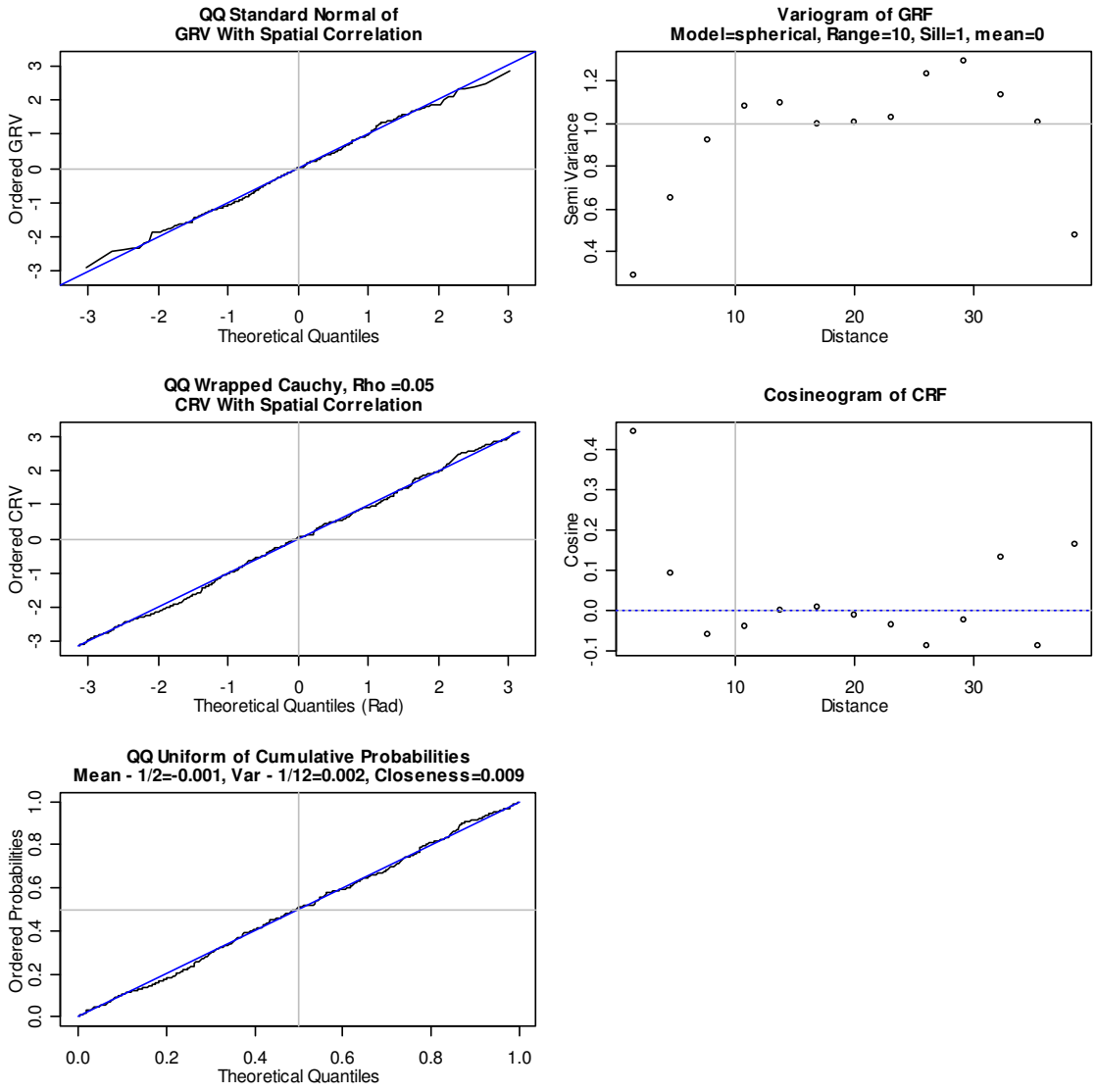

Figure D-13. Evaluation of a Wrapped Cauchy CRF, $\rho = 0.05$, Overfit, Range $r = 10$. The linearity of the QQ plots indicates that the distributional fits are close. The spatial plots on the right show agreement with the desired spatial characteristics (range r =10, sill=0).

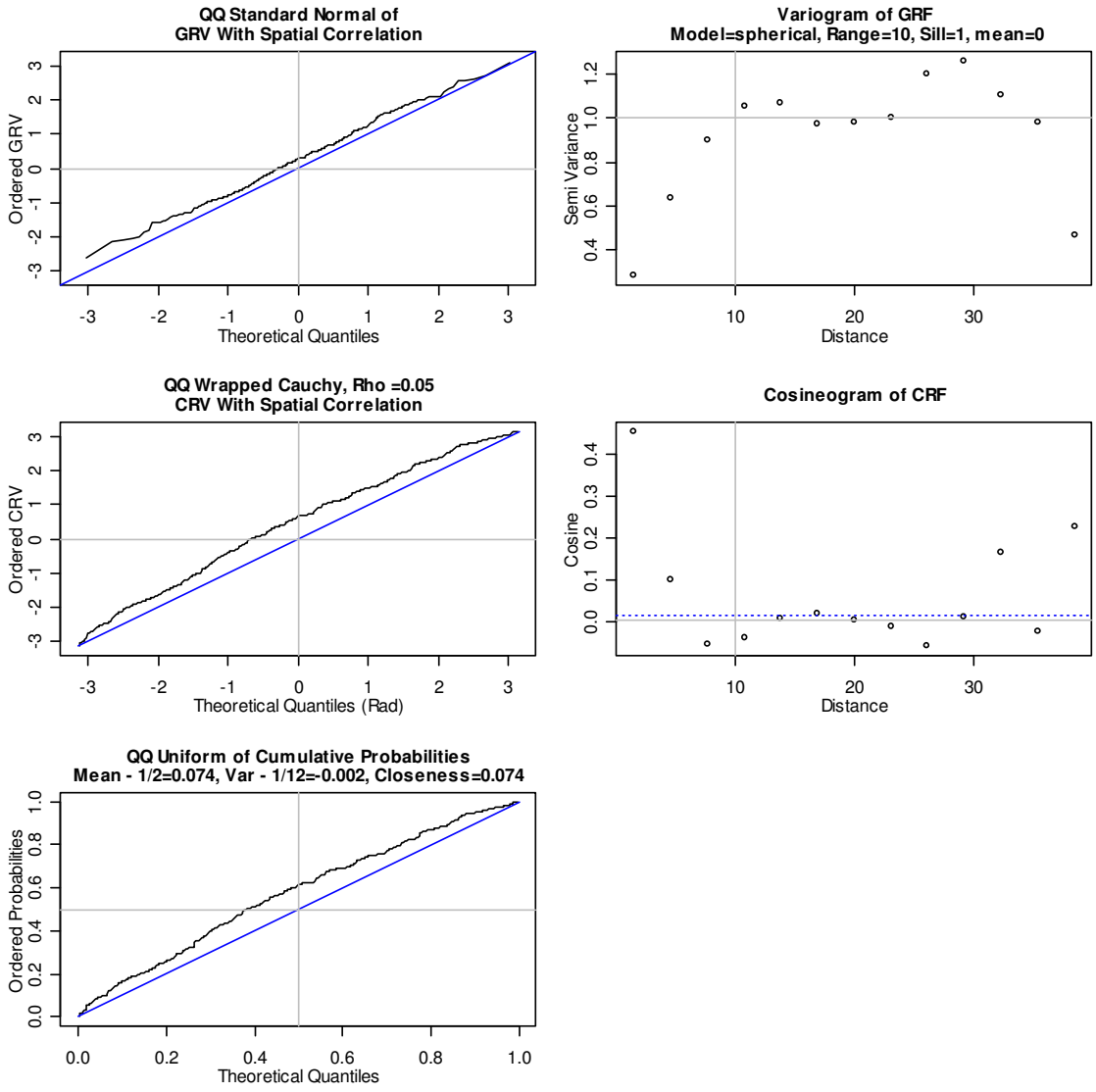

Figure D-14. Evaluation of a Wrapped Cauchy CRF, $\rho = 0.05$, Range $r = 10$. The lack of linearity of the QQ plots is due to typical sampling variation. The spatial plots on the right show agreement with the desired spatial characteristics (range r =10, sill=0).

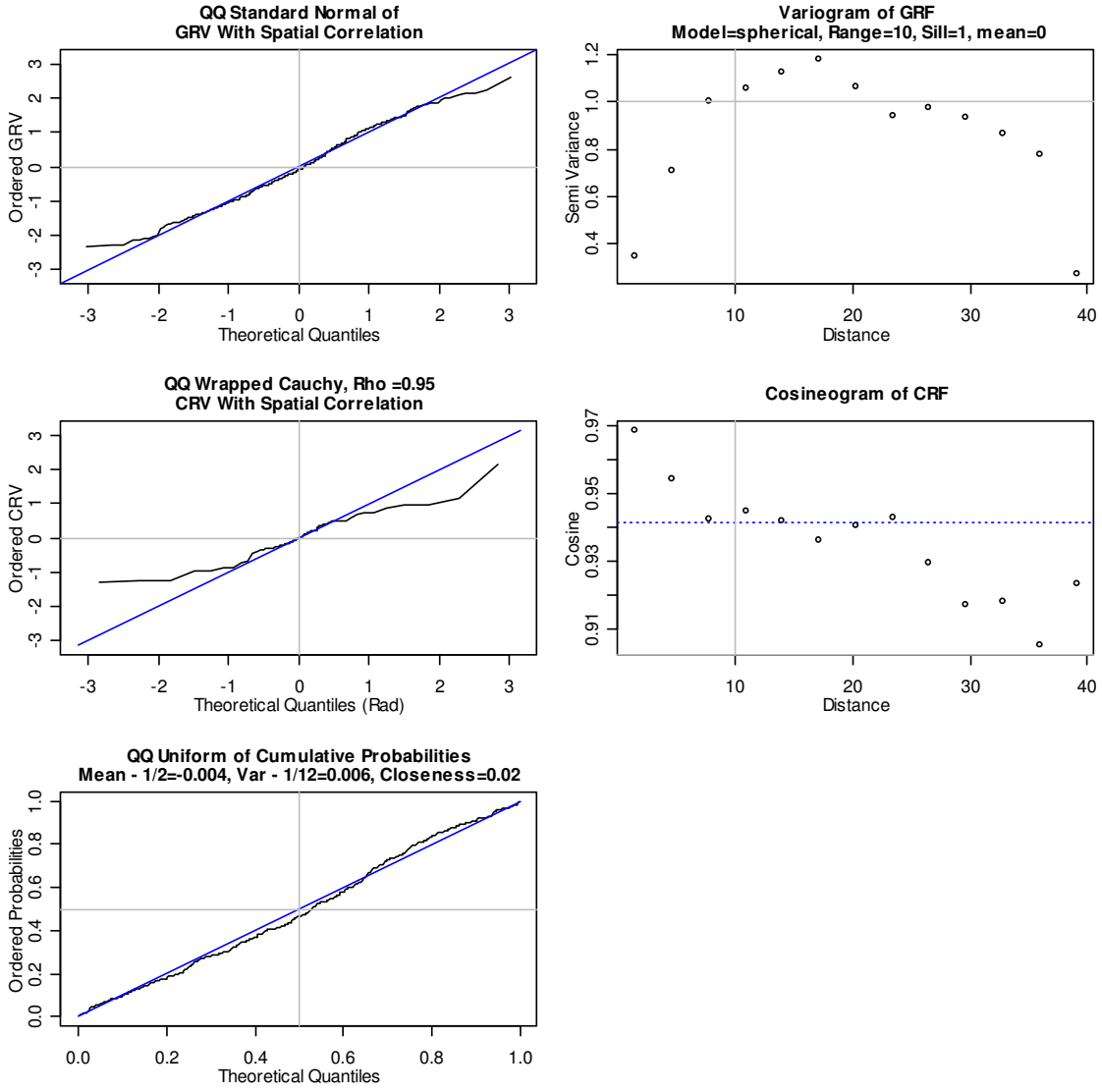

Figure D-15. Evaluation of a Wrapped Cauchy CRF, $\rho = 0.95$, Overfit, Range $r = 10$
The QQ plots show that the GRV and uniform samples (cumulative probabilities) were a close fit to the corresponding distributions, but the wrapped Cauchy circular sample at high ρ had less fit than the other circular samples. Since the linear Cauchy distribution gives samples with poor fit, it is not surprising that sampling from the linear Cauchy wrapped on a circle, or the wrapped Cauchy distribution, also gives samples with poor fit. The cosineogram on the right indicates a range of about 10 and a sill of about 0.94, which is slightly higher than ρ^2.

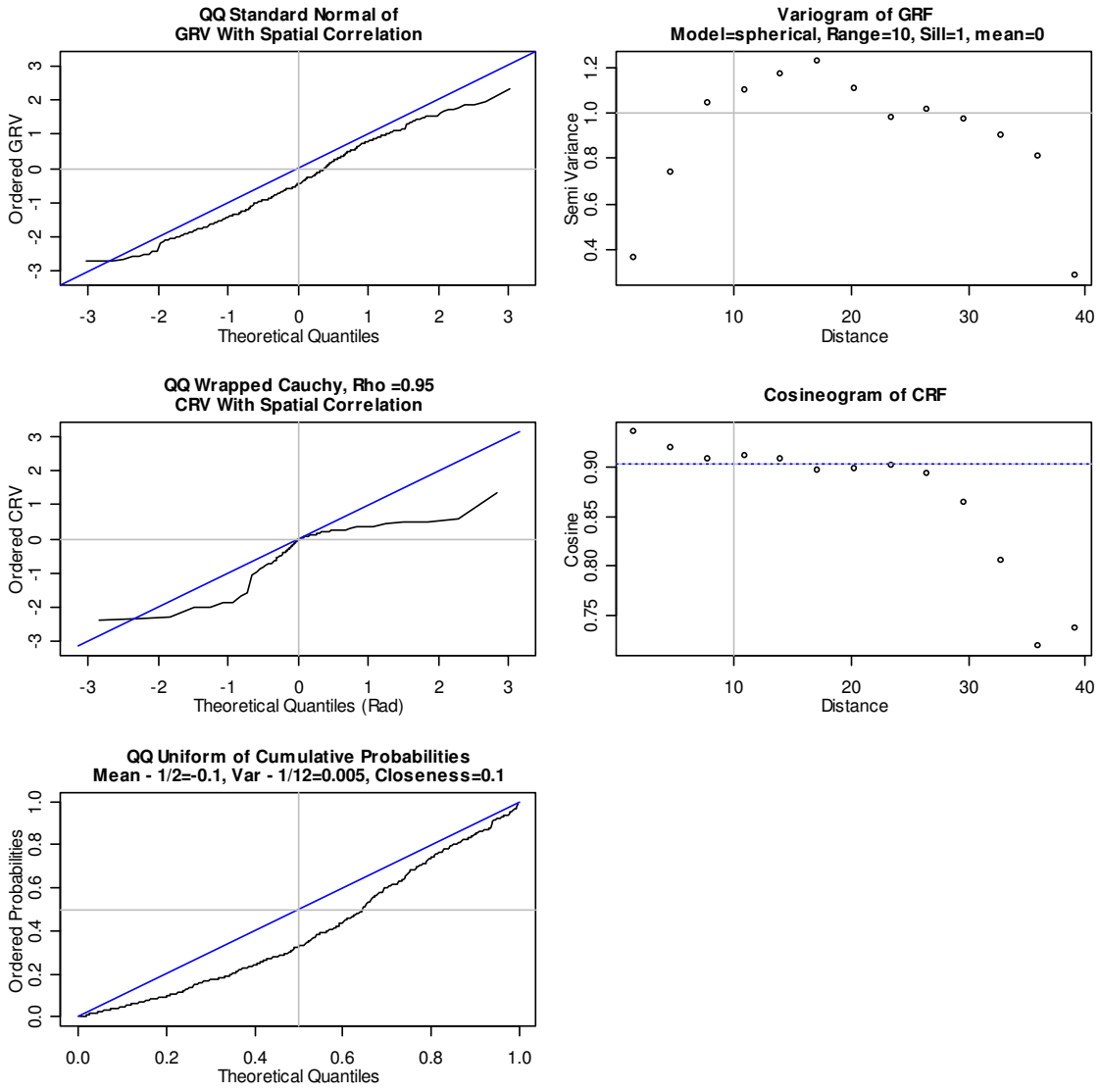

Figure D-16. Evaluation of a Wrapped Cauchy CRF, $\rho = 0.95$, Range $r = 10$. The lack of linearity of the QQ plots is due to typical sampling variation. The wrapped Cauchy circular sample at high ρ had poor fit similar to Figure D-15. The cosineogram on the right shows agreement with the desired spatial characteristics (range r =10, sill=$0.9 = \rho^2$).

The spatial properties of Figures D-1 to D-16 were scored and tabulated in Table D-1. The figures were scored based on the assessments in the figure captions:

- Good = Figure caption contains “agreement with the desired spatial characteristics”
- OK = Range and sill quantified
- Poor = Figure caption contains “sill is not well defined”.

Table D-1. Spatial Property Scores of Figures D-1 to D-16

Overfit	Good	OK	Poor
Yes	3	4	1
No	3	3	2

Appendix E

Derivations of the CDF Formulae for Support $[0, 2\pi)$

In Chapter 5, a Gaussian random field (GRF) is mapped to a circular random field (CRF) via the CDFs. The CDFs are derived for four circular distributions with $G_\Theta(\theta)$ the cumulative probability distribution function of Θ, ρ the mean resultant length parameter and κ the concentration parameter for the von Mises distribution, and $0 \le \theta_1 < \theta_2 < 2\pi$. To simplify calculation, the mean direction is assumed to be 0. With exception to the circular uniform distribution, the mean direction of the CRF may be set to an arbitrary direction by adding the direction minus the sample mean direction to the direction of each of the observations. Probability density functions were obtained from Mardia (1972), Fisher (1993), and Jammalamadaka and Sengupta (2001). The derived cumulative distribution function (CDF) formulae of Appendix E will be verified by integration over the support $[0, 2\pi)$ in Appendix F, and mapped to support $[-\pi, +\pi)$ in Appendices G and H. . The CDFs will be denoted $G_U(\theta)$ for the uniform, $G_T(\theta;\rho)$ for the triangular, $G_C(\theta;\rho)$ for the cardioid, $G_{vM}(\theta;\rho)$ for the von Mises, and $G_{WC}(\theta;\rho)$ for the wrapped Cauchy distributions.

E.1 Cardioid

The probability density function (PDF) is given in Mardia (1972, p. 51, eq. 3.4.11) and the CDF is given in Fisher (1993, p. 45, eq. 3.22). With $0 < \rho \le \frac{1}{2}$,

$$\begin{aligned} G_C(\theta_2;\rho) - G_C(\theta_1;\rho) &= \int_{\theta_1}^{\theta_2} \frac{1}{2\pi}(1 + 2\rho\cos(\theta))d\theta \\ &= \frac{1}{2\pi}\int_{\theta_1}^{\theta_2} d\theta + \frac{1}{2\pi}\int_{\theta_1}^{\theta_2} 2\rho\cos(\theta)d\theta \\ &= \frac{\theta_2 - \theta_1}{2\pi} + \frac{2\rho}{2\pi}\sin(\theta)\Big|_{\theta_1}^{\theta_2} \\ &= \frac{\theta_2 - \theta_1 + 2\rho(\sin(\theta_2) - \sin(\theta_1))}{2\pi} \Rightarrow \end{aligned}$$

$$G_C(\theta_2;\rho) - G_C(\theta_1;\rho) = \frac{\theta_2 - \theta_1 + 2\rho(\sin(\theta_2) - \sin(\theta_1))}{2\pi}. \quad \text{(E.1)}$$

E.2 Triangular

The PDF was obtained from Mardia (1972, p. 51, eq. (3.4.13). The CDF and derivation were not found in the cited texts, and may be a new result. With $0 < \rho \le 4/\pi^2$,

$$\begin{aligned} G_T(\theta_2;\rho) - G_T(\theta_1;\rho) &= \int_{\theta_1}^{\theta_2} \frac{1}{8\pi}\left(4 - \pi^2\rho + 2\pi\rho\left|\pi - \theta\right|\right)d\theta \\ &= \frac{1}{8\pi}\int_{\theta_1}^{\theta_2}\left(4 - \pi^2\rho\right)d\theta + \frac{1}{8\pi}\int_{\theta_1}^{\theta_2} 2\pi\rho\left|\pi - \theta\right| d\theta \\ &= \frac{\left(4 - \pi^2\rho\right)}{8\pi}(\theta_2 - \theta_1) + \frac{\rho}{4}\int_{\theta_1}^{\theta_2}\left|\pi - \theta\right| d\theta \Rightarrow \end{aligned}$$

Case 1, $0 \le \theta_1 < \theta_2 \le \pi$

$$= \frac{\left(4-\pi^2\rho\right)}{8\pi}(\theta_2-\theta_1)+\frac{\rho}{4}\int_{\theta_1}^{\theta_2}(\pi-\theta)\,d\theta$$
$$= \frac{\left(4-\pi^2\rho\right)}{8\pi}(\theta_2-\theta_1)+\frac{\rho}{4}\left(\pi\theta-\tfrac{1}{2}\theta^2\right)\Big|_{\theta_1}^{\theta_2}$$
$$= \frac{\left(4-\pi^2\rho\right)}{8\pi}(\theta_2-\theta_1)+\frac{\pi\rho}{4}\theta\Big|_{\theta_1}^{\theta_2}-\frac{\rho}{8}\theta^2\Big|_{\theta_1}^{\theta_2}$$
$$= \frac{\left(4-\pi^2\rho\right)}{8\pi}(\theta_2-\theta_1)+\frac{\pi\rho}{4}(\theta_2-\theta_1)-\frac{\rho}{8}\left(\theta_2^2-\theta_1^2\right)$$
$$= \left(\frac{\left(4-\pi^2\rho\right)}{8\pi}+\frac{2\pi^2\rho}{8\pi}-\frac{\pi\rho}{8\pi}(\theta_2+\theta_1)\right)(\theta_2-\theta_1)$$
$$= \left(\frac{4+\pi^2\rho-\pi\rho\left(\theta_2+\theta_1\right)}{8\pi}\right)(\theta_2-\theta_1)\Rightarrow$$

$$G_T(\theta_2;\rho)-G_T(\theta_1;\rho)=\left(\frac{4+\pi^2\rho-\pi\rho(\theta_2+\theta_1)}{8\pi}\right)(\theta_2-\theta_1) \qquad \text{(E.2)}$$

Case 2, $\pi \le \theta_1 < \theta_2 \le 2\pi$

$$= \frac{\left(4-\pi^2\rho\right)}{8\pi}(\theta_2-\theta_1)+\frac{\rho}{4}\int_{\theta_1}^{\theta_2}\left|\pi-\theta\right|d\theta$$
$$= \frac{4-\pi^2\rho}{8\pi}(\theta_2-\theta_1)+\frac{\rho}{4}\int_{\theta_1}^{\theta_2}(\theta-\pi)\,d\theta$$
$$= \frac{4-\pi^2\rho}{8\pi}(\theta_2-\theta_1)+\frac{\rho}{4}\tfrac{1}{2}\theta^2\Big|_{\theta_1}^{\theta_2}-\frac{\pi\rho}{4}\theta\Big|_{\theta_1}^{\theta_2}$$
$$= \frac{4-\pi^2\rho}{8\pi}(\theta_2-\theta_1)+\frac{\rho}{8}\left(\theta_2^2-\theta_1^2\right)-\frac{\pi\rho}{4}(\theta_2-\theta_1)$$
$$= \left\{\frac{4-\pi^2\rho}{8\pi}-\frac{2\pi^2\rho}{8\pi}\right\}(\theta_2-\theta_1)+\frac{\rho}{8}(\theta_2+\theta_1)(\theta_2-\theta_1)$$
$$= \frac{4-3\pi^2\rho+\pi\rho\left(\theta_2+\theta_1\right)}{8\pi}(\theta_2-\theta_1)\Rightarrow$$

$$G_T(\theta_2;\rho)-G_T(\theta_1;\rho)=\frac{4-3\pi^2\rho+\pi\rho\left(\theta_2+\theta_1\right)}{8\pi}(\theta_2-\theta_1) \qquad \text{(E.3)}$$

Case 3, $0 \le \theta_1 < \pi \le \theta_2 \le 2\pi$

$$= \left(\frac{4-\pi^2\rho}{8\pi}\right)(\theta_2-\theta_1) + \frac{\rho}{4}\int_{\theta_1}^{\pi}(\pi-\theta)\,d\theta + \frac{\rho}{4}\int_{\pi}^{\theta_2}(\theta-\pi)\,d\theta$$

$$= \left(\frac{4-\pi^2\rho}{8\pi}\right)(\theta_2-\theta_1) + \frac{\rho}{4}\left(\pi\theta - \tfrac{1}{2}\theta^2\right)\Big|_{\theta=\theta_1}^{\theta=\pi} + \frac{\rho}{4}\left(\tfrac{1}{2}\theta^2 - \pi\theta\right)\Big|_{\theta=\pi}^{\theta=\theta_2}$$

$$= \left(\frac{4-\pi^2\rho}{8\pi}\right)(\theta_2-\theta_1) + \frac{\rho}{4}\left(\pi\pi - \tfrac{1}{2}\pi^2\right) - \frac{\rho}{4}\left(\pi\theta_1 - \tfrac{1}{2}\theta_1^2\right) + \frac{\rho}{4}\left(\tfrac{1}{2}\theta_2^2 - \pi\theta_2\right) - \frac{\rho}{4}\left(\tfrac{1}{2}\pi^2 - \pi\pi\right)$$

$$= \left(\frac{4-\pi^2\rho}{8\pi}\right)(\theta_2-\theta_1) + \frac{\rho}{4}\tfrac{1}{2}\pi^2 - \frac{\rho}{4}\left(\pi - \tfrac{1}{2}\theta_1\right)\theta_1 + \frac{\rho}{4}\left(\tfrac{1}{2}\theta_2 - \pi\right)\theta_2 + \frac{\rho}{4}\tfrac{1}{2}\pi^2$$

$$= \left(\frac{4-\pi^2\rho}{8\pi}\right)(\theta_2-\theta_1) - \frac{\pi\rho\theta_1}{4} + \frac{\rho}{4}\tfrac{1}{2}\theta_1^2 + \frac{\rho}{4}\tfrac{1}{2}\theta_2^2 - \frac{\pi\rho}{4}\theta_2 + \pi^2\frac{\rho}{4}$$

$$= \left(\frac{4-\pi^2\rho}{8\pi}\right)(\theta_2-\theta_1) - \frac{2\pi^2\rho(\theta_1+\theta_2)}{8\pi} + \frac{\pi\rho}{8\pi}\left(\theta_1^2+\theta_2^2\right) + \pi^2\frac{\rho}{4}$$

$$= \frac{(4-\pi^2\rho)(\theta_2-\theta_1) - 2\pi^2\rho(\theta_1+\theta_2) + \pi\rho\left(\theta_1^2+\theta_2^2\right)}{8\pi} + \pi^2\frac{\rho}{4} \Rightarrow$$

$$G_T(\theta_2;\rho) - G_T(\theta_1;\rho) = \frac{(4-\pi^2\rho)(\theta_2-\theta_1) - 2\pi^2\rho(\theta_1+\theta_2) + \pi\rho\left(\theta_1^2+\theta_2^2\right)}{8\pi} + \frac{\pi^2\rho}{4}. \quad \text{(E.4)}$$

E.3 Uniform

$$G_U(\theta_2) - G_U(\theta_1) = \int_{\theta_1}^{\theta_2}\frac{1}{2\pi}\,d\theta$$
$$= \frac{1}{2\pi}\theta\Big|_{\theta_1}^{\theta_2}$$
$$= (\theta_2-\theta_1)/(2\pi) \Rightarrow$$

$$G_U(\theta_2) - G_U(\theta_1) = (\theta_2-\theta_1)/(2\pi) \quad \text{(E.5)}$$

E.4 von Mises

The CDF for the von Mises distribution is not derived because CircStats provides the function pvm for the von Mises CDF.

E.5 Wrapped Cauchy

The PDF was obtained from Mardia (1972, p. 56, eq. 3.4.33). The following form of the CDF and its derivation were not found in the referenced texts, and may be a new result. With $0 < \rho < 1$,

$$
\begin{aligned}
G_{WC}(\theta_2;\rho) - G_{WC}(\theta_1;\rho) &= \int_{\theta_1}^{\theta_2} \frac{1}{2\pi}\left[1 + 2\sum_{k=1}^{\infty}\rho^k \cos(k\theta)\right] d\theta \\
&= \int_{\theta_1}^{\theta_2}\left[\frac{1}{2\pi} + \frac{1}{\pi}\rho\cos(\theta) + \frac{1}{\pi}\sum_{k=2}^{\infty}\rho^k\cos(k\theta)\right] d\theta \\
&= \frac{1}{2\pi}\int_{\theta_1}^{\theta_2} d\theta + \frac{\rho}{\pi}\int_{\theta_1}^{\theta_2}\cos(\theta)d\theta + \frac{1}{\pi}\int_{\theta_1}^{\theta_2}\left[\sum_{k=2}^{\infty}\rho^k\cos(k\theta)\right] d\theta \\
&= \frac{\theta_2 - \theta_1}{2\pi} + \frac{\rho}{\pi}(\sin(\theta_2) - \sin(\theta_1)) + \frac{1}{\pi}\sum_{k=2}^{\infty}\rho^k\frac{1}{k}\int_{\theta_1}^{\theta_2}\cos(k\theta)\, k d\theta \\
&= \frac{\theta_2 - \theta_1 + 2\rho(\sin(\theta_2) - \sin(\theta_1))}{2\pi} + \frac{1}{\pi}\sum_{k=2}^{\infty}\rho^k\frac{1}{k}(\sin(k\theta_2) - \sin(k\theta_1)) \Rightarrow
\end{aligned}
$$

$$
\begin{aligned}
G_{WC}(\theta_2;\rho) - G_{WC}(\theta_1;\rho) &= \frac{\theta_2 - \theta_1 + 2\rho(\sin(\theta_2) - \sin(\theta_1))}{2\pi} \\
&\quad + \frac{1}{\pi}\sum_{k=2}^{\infty}\rho^k\frac{1}{k}(\sin(k\theta_2) - \sin(k\theta_1)).
\end{aligned} \tag{E.6}
$$

Appendix F

Verification by Evaluation of the CDF Formulae with Support $[0, 2\pi)$

F.1 Cardioid

$$G_C(\theta = 2\pi;\rho) - G_C(\theta = 0;\rho) \overset{(E.1)}{=} \left\{ \frac{\theta_2 - \theta_1 + 2\rho(\sin(\theta_2) - \sin(\theta_1))}{2\pi} \right\} \Bigg|_{\theta_1=0}^{\theta_2=2\pi}$$

$$= \frac{2\pi - 0 + 2\rho(\sin(2\pi) - \sin(0))}{2\pi}$$

$$= \frac{2\pi + 2\rho(0 - 0)}{2\pi}$$

$$= 1 \Rightarrow$$

$$G_C(\theta = 2\pi;\rho) - G_C(\theta = 0;\rho) = 1$$

F.2 Triangular

Case 1, $0 \le \theta_1 < \theta_2 \le \pi$

$$G_T(\theta = \pi;\rho) - G_T(\theta = 0;\rho) \overset{(E.2)}{=} \left\{ \left(\frac{4 + \pi^2\rho - \pi\rho(\theta_2 + \theta_1)}{8\pi} \right)(\theta_2 - \theta_1) \right\} \Bigg|_{\theta_1=0}^{\theta_2=\pi}$$

$$= \left(\frac{4 + \pi^2\rho - \pi\rho(\pi + 0)}{8\pi} \right)(\pi - 0)$$

$$= \left(\frac{4 + \pi^2\rho - \pi\rho(\pi)}{8\pi} \right)\pi$$

$$= 0.5 \Rightarrow$$

$$G_T(\theta = \pi;\rho) - G_T(\theta = 0;\rho) = 0.5$$

Case 2, $\pi \le \theta_1 < \theta_2 \le 2\pi$

$$G_T(\theta = 2\pi;\rho) - G_T(\theta = \pi;\rho) \overset{(E.3)}{=} \left\{ \frac{4 - 3\pi^2\rho + \pi\rho(\theta_2 + \theta_1)}{8\pi}(\theta_2 - \theta_1) \right\} \Bigg|_{\theta_1=\pi}^{\theta_2=2\pi}$$

$$= \frac{4 - 3\pi^2\rho + \pi\rho(2\pi + \pi)}{8\pi}(2\pi - \pi)$$

$$= \frac{4 - 3\pi^2\rho + \pi\rho(3\pi)}{8\pi}(\pi)$$

$$= 0.5 \Rightarrow$$

$$G_T(\theta = 2\pi;\rho) - G_T(\theta = \pi;\rho) = 0.5$$

Case 3, $0 \le \theta_1 < \pi \le \theta_2 < 2\pi$

$$G_T(\theta = 2\pi;\rho) - G_T(\theta = 0;\rho) \overset{(E.4)}{=} \left\{ \frac{(4 - \pi^2\rho)(\theta_2 - \theta_1) - 2\pi^2\rho(\theta_1 + \theta_2) + \pi\rho(\theta_1^2 + \theta_2^2)}{8\pi} + \frac{\pi^2\rho}{4} \right\} \Bigg|_{\theta_1=0}^{\theta_2=2\pi}$$

$$= \frac{(4 - \pi^2\rho)(2\pi - 0) - 2\pi^2\rho(0 + 2\pi) + \pi\rho(0^2 + 4\pi^2)}{8\pi} + \frac{\pi^2\rho}{4}$$

$$= \frac{(8\pi - 2\pi^3\rho) - 4\pi^3\rho + 4\pi^3\rho}{8\pi} + \frac{2\pi^3\rho}{8\pi}$$

$$= \frac{8\pi - 2\pi^3\rho + 2\pi^3\rho}{8\pi}$$

$$= 1 \Rightarrow$$

$$G_T(\theta = 2\pi;\rho) - G_T(\theta = 0;\rho) = 1$$

F.3 Uniform

$$G_U(\theta = 2\pi) - G_U(\theta = 0) \overset{(E.5)}{=} \frac{\theta_2 - \theta_1}{2\pi} \Bigg|_{\theta_1=0}^{\theta_2=2\pi}$$

$$= \frac{2\pi - 0}{2\pi}$$

$$= 1 \Rightarrow$$

$$G_U(\theta = 2\pi) - G_U(\theta = 0) = 1$$

F.4 Von Mises

See E.4.

F.5 Wrapped Cauchy

$$G_{WC}(\theta = 2\pi;\rho) - G_{WC}(\theta = 0;\rho) \overset{(E.6)}{=} \left\{ \frac{\theta_2 - \theta_1 + 2\rho(\sin(\theta_2) - \sin(\theta_1))}{2\pi} + \frac{1}{\pi}\sum_{k=2}^{\infty} \rho^k \frac{1}{k}(\sin(k\theta_2) - \sin(k\theta_1)) \right\} \Bigg|_{\theta_1=0}^{\theta_2=2\pi}$$

$$\overset{F.2}{=} 1 + \frac{1}{\pi}\sum_{k=2}^{\infty} \rho^k \frac{1}{k}(\sin(k2\pi) - \sin(k0))$$

$$= 1 + \frac{1}{\pi}\sum_{k=2}^{\infty} \rho^k \frac{1}{k}(0 - 0)$$

$$= 1$$

$$G_{WC}(\theta = 2\pi;\rho) - G_{WC}(\theta = 0;\rho) = 1$$

Appendix G

Modification of the PDF and CDF Formulae for Rotated Support $[-\pi, +\pi)$

In Appendices G and H, the CDF formulae of Appendix E will be modified to rotate the support from $[0, 2\pi)$ to $[-\pi, +\pi)$ radians on the unit circle. In Appendix G, the PDF formulae will also be modified to rotate the support from $[0, 2\pi)$ to $[-\pi, +\pi)$.

Rotation of the CDF support is required to map a GRV to a CRV with mean direction 0 (Chapter 5, Section 5.3). Unlike the CDF of a linear random variable (RV), the circular CDF does not have a single origin. Let the support be $[-\pi, +\pi)$. Then, by means of the CDF – Inverse CDF transformation (Figure 5-2), the most negative values of the standard GRV map to the most negative values of a CRV, the modes coincide, and the most positive values of the GRV map to the most positive values of the CRV. Thus, the circular CDF has $G_\Theta(\theta = -\pi) = 0$, $G_\Theta(\theta = 0) = 0.5$, and $G_\Theta(\theta = \pi) = 1.0$.

The uniform PDF is $g(\theta) = 1/2\pi$ for all angles. Hence, it is independent of the choice of support, and the same for both supports. The cardioid, von Mises, and wrapped Cauchy distributions are functions of $\cos(\theta)$. To transform the part of the support $\pi \le \theta < 2\pi$ to the corresponding part $-\pi \le \phi < 0$, let $\theta = \phi + 2\pi$. Then, $\cos(\theta) = \cos(\phi + 2\pi) = \cos(\phi)\underbrace{\cos(2\pi)}_{1} - \sin(\phi)\underbrace{\sin(2\pi)}_{0} = \cos(\phi) \Rightarrow g(\theta) = g(\phi)$. Thus, the circular PDF for the uniform, cardioid, von Mises, and wrapped Cauchy distributions do not change with rotated support. For $0 \le \theta < \pi$, the PDF of the triangular distribution is $g(\theta) = \frac{1}{8\pi}\left(4 - \pi^2\rho + 2\pi\rho(\pi - \theta)\right)$. For the part of the rotated support $-\pi \le \phi < 0$, $g(\theta) = \frac{1}{8\pi}\left(4 - \pi^2\rho + 2\pi\rho(\theta - \pi)\right) = \frac{1}{8\pi}\left(4 - \pi^2\rho + 2\pi\rho(\phi + 2\pi - \pi)\right) = \frac{1}{8\pi}\left(4 - \pi^2\rho + 2\pi\rho(\phi + \pi)\right)$. This is given in Table 5-1 with $\delta = \pi + \theta, -\pi \le \theta < 0$, and $\delta = \pi - \theta, 0 \le \theta < \pi$.

G.1 Cardioid

$$G_C(\theta_2;\rho) - G_C(\theta_1;\rho) \overset{(E.1)}{=} \frac{\theta_2 - \theta_1 + 2\rho(\sin(\theta_2) - \sin(\theta_1))}{2\pi}$$

$$\overset{\text{By Inspection}}{\Rightarrow} \quad G_C(\theta;\rho) = \begin{cases} \dfrac{\theta + \pi + 2\rho\sin(\theta + 2\pi)}{2\pi}, & -\pi \le \theta < 0 \\ \dfrac{\theta + \pi + 2\rho\sin(\theta)}{2\pi}, & 0 \le \theta \le \pi \end{cases}$$

$$= \frac{\theta + \pi + 2\rho\sin(\theta)}{2\pi}, \; -\pi \le \theta \le \pi$$

$$G_C(\theta;\rho) = \frac{\theta + \pi + 2\rho\sin(\theta)}{2\pi}, \; -\pi \le \theta \le \pi \qquad \text{(G.1)}$$

Figure G-1, which verifies the cardioid CDF with support $[-\pi, +\pi)$, was plotted using the following R code:

```
par(mai=c(.8,.75,.1,.1)); r<-0.3
theta <- seq(-pi, pi, length=201)
GC <- (theta + pi + 2*r*sin(theta))/(2*pi)
plot(theta, GC, ty="l")
```

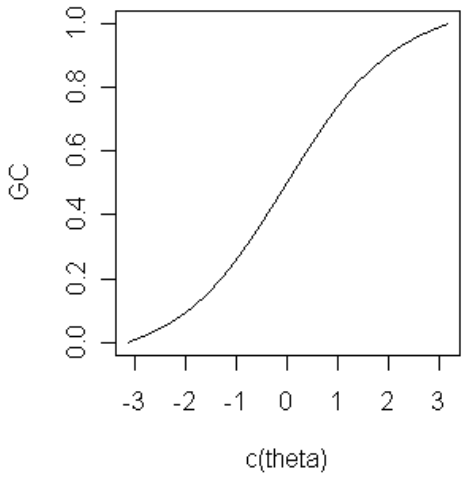

Figure G-1. Visual Verification of Cardioid CDF, $\rho = 0.30$, Support $[-\pi, +\pi)$ Radians. Slope is changing as expected with maximum slope occurring at zero radians.

G.2 Triangular

$$G_T(\theta_2;\rho)-G_T(\theta_1;\rho)\overset{(E.2)(E.3)}{=}\begin{cases}\left(\dfrac{4+\pi^2\rho-\pi\rho(\theta_2+\theta_1)}{8\pi}\right)(\theta_2-\theta_1), & 0\le\theta_1<\theta_2\le\pi\\ \dfrac{4-3\pi^2\rho+\pi\rho(\theta_2+\theta_1)}{8\pi}(\theta_2-\theta_1), & \pi\le\theta_1<\theta_2<2\pi\end{cases}$$

$$\overset{inspection}{\Rightarrow}$$

$$G_T(\theta;\rho)=\begin{cases}\dfrac{4-3\pi^2\rho+\pi\rho(\theta+3\pi)}{8\pi}(\theta+\pi), & -\pi\le\theta<0\\ 0.5+\left[\dfrac{4+\pi^2\rho-\pi\rho\theta}{8\pi}\right]\theta, & 0\le\theta\le\pi\end{cases}\qquad\text{(G.2)}$$

Figure G-2, which verifies the triangular CDF with support $[-\pi,+\pi)$, was plotted using the following R code:

```
par(mai=c(.8,.75,.1,.1)); r<-0.3
theta1 <- seq(-pi,0,length=100); theta1 <- theta1[-100]; theta2 <- seq(0,pi,length=100)
GT1 <- (4-3*pi^2*r + pi*r*(theta1+ 3*pi))*(theta1+pi)/(8*pi)
GT2 <- 0.5 + (4 + pi^2*r - pi*r*theta2)*theta2/(8*pi)
plot(c(theta1,theta2), c(GT1, GT2), ty="l")
```

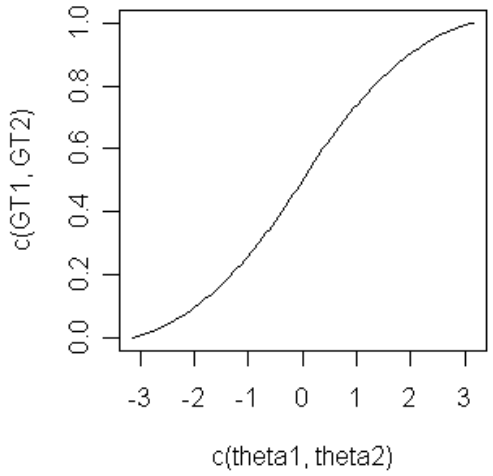

Figure G-2. Visual Verification of Triangular CDF, $\rho=0.30$, Support $[-\pi,+\pi)$ Radians. Slope is changing as expected with maximum slope occurring at zero radians.

G.3 Uniform

$$G_U(\theta_2) - G_U(\theta_1) \overset{(E.5)}{=} \frac{\theta_2 - \theta_1}{2\pi} \overset{inspection}{\Rightarrow}$$

$$G_U(\theta) = \frac{\theta + \pi}{2\pi}, \quad -\pi \le \theta \le \pi \tag{G.3}$$

G.4 von Mises

The von Mises cumulative probabilities computed via function pvm in R package CircStats (Lund and Agostinelli 2006):

```
> pvm(theta = -pi, mu=0, kappa=1)
[1] 0.5
> pvm(theta = -.0000001, mu=0, kappa=1)
[1] 1
> pvm(theta = 0, mu=0, kappa=1)
[1] 0
> pvm(theta = pi, mu=0, kappa=1)
[1] 0.5
> pvm(theta = 2*pi, mu=0, kappa=1)
[1] 0

> pvm(theta = 2*pi -.0000001, mu = 0, kappa = 1)
[1] 1
```

$\overset{inspection}{\Rightarrow}$

$$G_{vM}(\theta;\kappa) = \begin{cases} pvm(\theta, mu = 0, kappa = k) - 0.5, & -\pi \le \theta < 0 \\ pvm(\theta, mu = 0, kappa = k) + 0.5, & 0 \le \theta \le \pi \end{cases} \tag{G.4}$$

Figure G-3, which verifies the von Mises CDF with support $[-\pi, +\pi)$, was plotted using the following R code:

```
require(CircStats)
r<-0.3; k<-A1inv(r)
par(mai=c(.8,.75,.1,.1))
theta1 <- seq(-pi,0,length=100); theta1 <- theta1[-100]; theta2 <- seq(0,pi,length=100)
GvM1 <- pvm(theta1, mu=0, kappa=k ) - 0.5
GvM2 <- pvm(theta2, mu=0, kappa=k ) + 0.5
plot(c(theta1,theta2), c(GvM1, GvM2), ty="l")
```

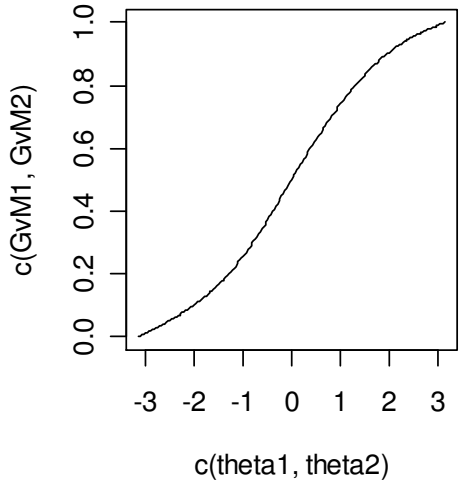

Figure G-3. Visual Verification of von Mises CDF, $\rho = 0.30$, Support $[-\pi, +\pi)$ Radians. Slope is changing as expected with maximum slope occurring at zero radians.

G.5 Wrapped Cauchy

Additional forms of the wrapped Cauchy CDF were discovered after the completion of Chapter 3. One of these forms is incorrect. Due to the complexity of the issues arising from the multiple forms of the wrapped Cauchy CDF, these forms will be treated in Appendix H.

Appendix H

Wrapped Cauchy CDF

H.1 Additional Forms of the CDF

H.1.1 Incorrect CDF

This distribution was introduced by Lévy (1939). (H.1) was taken from Mardia (1972, p. 57, eq. 3.4.36), and repeated in Fisher (1993, p. 46, 3.27). With $\mu = 0$, it is

$$G_{WC}(\theta;\rho) = \frac{1}{2\pi}\cos^{-1}\left(\frac{\left(1+\rho^2\right)\cos(\theta)-2\rho}{1+\rho^2-2\rho\cos(\theta)}\right), 0 \le \theta < 2\pi, \mu = 0. \tag{H.1}$$

(H.1) is plotted in Figure H-1 with the following code:

```
theta <- seq(0, 2*pi, length = 197); r <- 0.75 # rho
G <- acos(((1+r^2)*cos(theta)-2*r)/(1+r^2-2*r*cos(theta)))/(2*pi)
plot(theta, G, ty = "l", cex.lab=1.6, cex.axis=1.2)
```

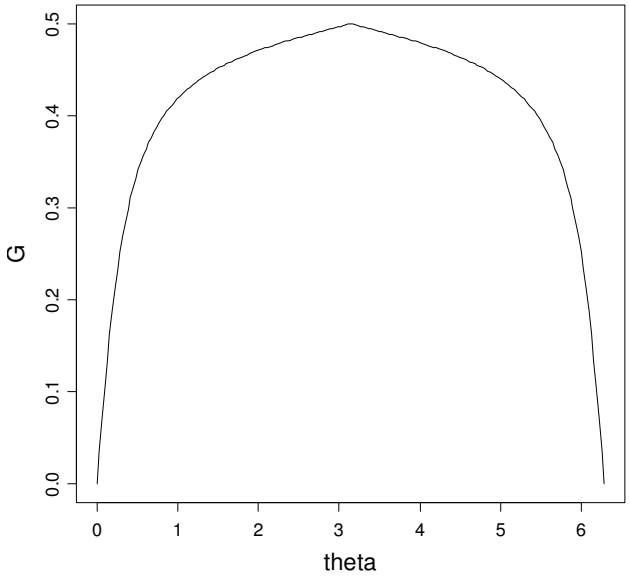

Figure H-1. Incorrect Wrapped Cauchy CDF, $\rho = 0.75$, Support $[0, 2\pi)$ Radians. A correct CDF is monotonic increasing.

H.1.2 WCACDF

WCACDF was obtained from National Institute of Standards and Technology (NIST), Statistical Engineering Division, Dataplot, at http://www.itl.nist.gov/div898/software/dataplot/refman2/auxillar/wcacdf.pdf, eq. Aux-326. With $\mu = 0$, it is

$$G_{WC}(\theta;\rho) = \begin{cases} \dfrac{\tan^{-1}\left(\dfrac{-\sin\left(\frac{\theta}{2}\right)-\rho\sin\left(\frac{\theta}{2}\right)}{-\cos\left(\frac{\theta}{2}\right)+\rho\cos\left(\frac{\theta}{2}\right)}\right)-\tan^{-1}\left(\dfrac{\sin\left(\frac{\theta}{2}\right)+\rho\sin\left(\frac{\theta}{2}\right)}{-\cos\left(\frac{\theta}{2}\right)+\rho\cos\left(\frac{\theta}{2}\right)}\right)}{2\pi} \equiv G_{WC1}, 0 \le \theta < \pi \\ 1 - G_{WC1}(2\pi - \theta;\rho), \pi < \theta < 2\pi. \end{cases} \quad \text{(H.2)}$$

They cite Johnson, Kotz, and Balakrishnan (1994), which is a principle reference for looking up details on distributions. (H.2), as shown in Figure H-2, was plotted with the following code:

```
theta1 <- seq(pi, 2*pi, length = 100); theta2 <- seq(0, pi, length = 100)
theta3 <- seq(-pi, 0, length = 100); r <- 0.75
G <- function(theta) {(atan((-1-r)*sin(.5*theta)/((-1+r)*cos(.5*theta)) )
        - atan( (1+r)*sin(.5*theta)/((r-1)*cos(.5*theta))))/(2*pi)}
plot(c(theta2, theta1), c(G(theta2), 1-G(2*pi-theta1)), ty = "l", cex.lab=1.6, cex.axis=1.2)
```

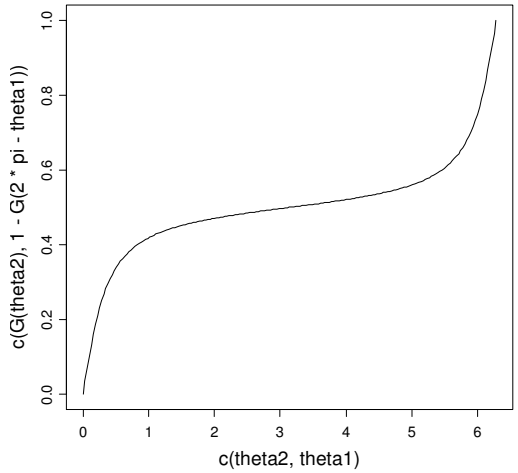

Figure H-2. Dataplot WCACDF of Wrapped Cauchy CDF, $\rho = 0.75$, Support $[0, 2\pi)$ Radians. The slope changes with maximum rate at zero radians as expected.

H.2 Alternate Forms with Support $[0, 2\pi)$

This section will modify the CDF formulae of Section H.1 and Appendix E, Section E.5 to facilitate evaluation. These circular CDFs, going counterclockwise, will have $G_{WC}(\theta=\pi;\rho)=0$, $G_{WC}(\theta=2\pi;\rho)=0.5$, $G_{WC}(\theta=0;\rho)=0.5$, and $G_{WC}(\theta=\pi;\rho)=1.0$.

H.2.1 Iterated

$$G_{WC}(\theta;\rho) \overset{(E.6)}{=} \begin{cases} 0.5+\dfrac{\theta+2\rho\sin(\theta)}{2\pi}+\dfrac{1}{\pi}\sum_{k=2}^{\infty}\rho^k\dfrac{1}{k}\sin(k\theta), 0\le\theta<\pi \\ -0.5+\dfrac{\theta+2\rho\sin(\theta)}{2\pi}+\dfrac{1}{\pi}\sum_{k=2}^{\infty}\rho^k\dfrac{1}{k}\sin(k\theta), \pi\le\theta<2\pi \end{cases} \tag{H.3}$$

H.2.2 Revised (H.1)

$$G_{WC}(\theta;\rho) \overset{(H.1)}{=} \begin{cases} 0.5+\dfrac{1}{2\pi}\cos^{-1}\left(\dfrac{\left(1+\rho^2\right)\cos(\theta)-2\rho}{1+\rho^2-2\rho\cos(\theta)}\right), 0\le\theta<\pi \\ 0.5-\dfrac{1}{2\pi}\cos^{-1}\left(\dfrac{\left(1+\rho^2\right)\cos(\theta)-2\rho}{1+\rho^2-2\rho\cos(\theta)}\right), \pi\le\theta<2\pi \end{cases} \tag{H.4}$$

H.2.3 WCACDF

$$F(\theta;\rho) \overset{(H.2)}{=} \frac{\tan^{-1}\left(\dfrac{-\sin\left(\frac{\theta}{2}\right)-\rho\sin\left(\frac{\theta}{2}\right)}{-\cos\left(\frac{\theta}{2}\right)+\rho\cos\left(\frac{\theta}{2}\right)}\right)-\tan^{-1}\left(\dfrac{\sin\left(\frac{\theta}{2}\right)+\rho\sin\left(\frac{\theta}{2}\right)}{-\cos\left(\frac{\theta}{2}\right)+\rho\cos\left(\frac{\theta}{2}\right)}\right)}{2\pi}$$

$$G_{WC}(\theta;\rho)=\begin{cases} 0.5+F(\theta;\rho), 0\le\theta<\pi \\ 0.5-F(2\pi-\theta;\rho), \pi\le\theta<2\pi \end{cases} \tag{H.5}$$

H.3 Evaluation of Alternate Forms

H.3.1 Forms of Wrapped Cauchy CDF Visually Indistinguishable

In Figure H-3, the circular CDFs are computed over $[\pi, 2\pi) \cup [0, \pi)$ and plotted over the equivalent support $[-\pi, +\pi)$ using the following R code:

```
theta1 <- seq(pi, 2*pi, length = 100); theta1 <- theta1[-100]
theta2 <- seq(0, pi, length = 100);    theta2 <- theta2[-100]
theta3 <- seq(-pi,0, length = 100);    theta3 <- theta3[-100]; r <- 0.75
# Iterated CDF with total 15 iterations
GI1 <- (theta1-pi+2*r*sin(theta1))/(2*pi); GI2 <- 0.5 + (theta2+2*r*sin(theta2))/(2*pi)
GI <- function(theta)
{ sum.iter <- 0; for (k in 2:15) { sum.iter <- sum.iter + (1/pi)*(r^k)*(1/k)*sin(k*theta)}
        return(sum.iter) }
GI1 <- GI1 + GI(theta1); GI2 <- GI2 + GI(theta2)
par(mai=c(.65,.6,.1,.1), mgp=c(2,1,0),cex.axis=.7, cex.lab=.8)
plot(c(theta3, theta2), c(GI1, GI2), ty = "l")
# Corrected wrapped Cauchy CDF
GM1 <- .5 - acos(((1+r^2)*cos(theta1)-2*r)/(1+r^2-2*r*cos(theta1)))/(2*pi)
GM2 <- .5 +acos(((1+r^2)*cos(theta2)-2*r)/(1+r^2-2*r*cos(theta2)))/(2*pi)
plot(c(theta3, theta2), c(GM1, GM2), ty = "l")
F <- function(theta) {(atan((-1-r)*sin(.5*theta)/((-1+r)*cos(.5*theta)) )
        - atan( (1+r)*sin(.5*theta)/((r-1)*cos(.5*theta))))/(2*pi)}
GD1 <- .5 - F(2*pi-theta1); GD2 <- F(theta2) + 0.5
plot(c(theta3, theta2), c(GD1, GD2), ty = "l")
```

In Figure H-3, the revised wrapped Cauchy CDF, WCACDF, and the iterative formula with 15 iterations are visually indistinguishable.

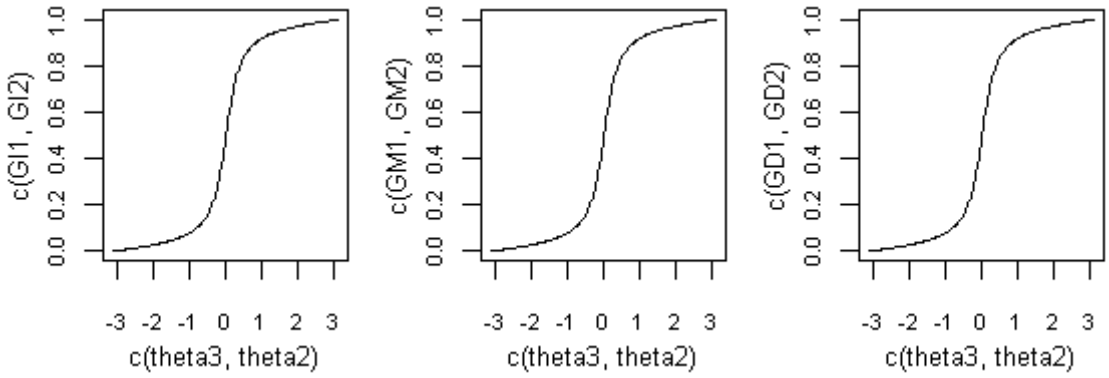

Figure H-3. Three Forms of the Wrapped Cauchy CDF, $\rho = 0.75$, Support $[-\pi, \pi)$ Radians. Visually, the three forms are indistinguishable.

H.3.2 Proximity of Alternative CDF Formulae

With 198 points, the revised CDF and WCACDF total absolute difference is about e-14. The iterated CDF achieves the similar accuracy when the number of iterations is increased to about 160 iterations.

```
# Compare iterative to WCACDF
sum(abs(c(GI1, GI2) – c(GD1,GD2)))
[1] 0.02960684

# Compare iterative to revised CDF
sum(abs(c(GI1, GI2) – c(GM1,GM2)))
[1] 0.02960684

# Compare WCACDF to revised CDF
sum(abs(c(GD1, GD2) – c(GM1,GM2)))
[1] 3.375078e-14
```

The accuracy of the iterated wrapped Cauchy CDF (H.3) depends on ρ and the number of iterations. As rho increases, the number of iterations must increase to maintain accuracy. The need for additional iterations at high rho (0.95) is demonstrated in Figure H-4, which was plotted with the following R code:

```
r <- 0.95; GI1 <- (theta1-pi+2*r*sin(theta1))/(2*pi); GI2 <- 0.5 + (theta2+2*r*sin(theta2))/(2*pi)
GI1 <- GI1 + GI(theta1); GI2 <- GI2 + GI(theta2); plot(c(theta3, theta2), c(GI1, GI2), ty = ”l”)
```

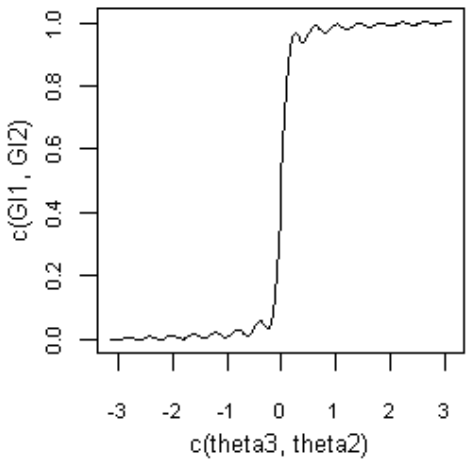

Figure H-4. Iterated Wrapped Cauchy CDF, $\rho = 0.95$, Support $[-\pi, \pi)$ Radians, 15 Iterations. The iterative form gets rough as $\rho \to 1$ and computation time increases.

H.4 Selected Form for Rotated Support $[-\pi, +\pi)$

The revised CDF (H.4) is more simple than the WCACDF (H.5), and does not have the inaccuracy of the iterative form (H.3) at high rho. Hence, the selected wrapped Cauchy CDF for support $[-\pi, +\pi)$ is:

$$G_{WC}(\theta;\rho) \overset{(H.4)}{=} \begin{cases} .5 - \frac{1}{2\pi}\cos^{-1}\left(\frac{(1+\rho^2)\cos(\theta)-2\rho}{1+\rho^2-2\rho\cos(\theta)}\right), -\pi \le \theta < 0 \\ .5 + \frac{1}{2\pi}\cos^{-1}\left(\frac{(1+\rho^2)\cos(\theta)-2\rho}{1+\rho^2-2\rho\cos(\theta)}\right), 0 \le \theta \le \pi. \end{cases} \quad \text{(H.6)}$$

(H.6), as shown in Figure H-5, was plotted with the following code:

```
par(mai=c(.8,.75,.1,.1))
r <- 0.75
theta1 <- seq(-pi,0, length = 100); theta1 <- theta1[-100]
theta2 <- seq(0, pi, length = 100)
GM1 <- .5 - acos(((1+r^2)*cos(theta1)-2*r)/(1+r^2-2*r*cos(theta1)))/(2*pi)
GM2 <- .5 +acos(((1+r^2)*cos(theta2)-2*r)/(1+r^2-2*r*cos(theta2)))/(2*pi)
plot(c(theta1, theta2), c(GM1, GM2), ty = "l")
```

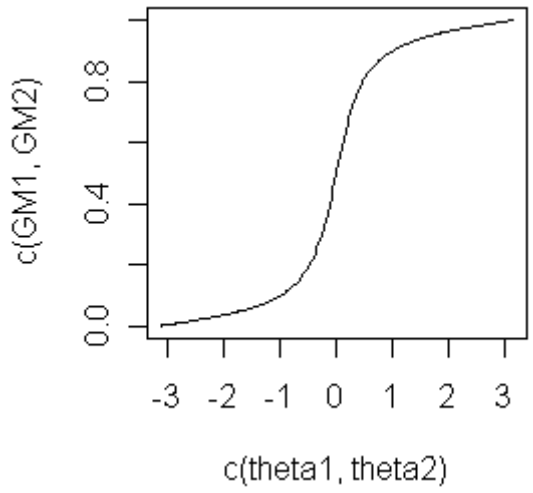

Figure H-5. Visual Verification of Wrapped Cauchy CDF, $\rho = 0.75$, Support $[-\pi, \pi)$ Radians. The slope changes with maximum rate at zero radians as expected.

Appendix I

Triangular Inverse CDF

The inverse CDF is computed in order to map a Gaussian random field to a circular random field according to the method of Chapter 5, Section 5.3. For the cumulative probability $u = F_Z(z(\boldsymbol{x}))$, and the triangular CDF $G_T(\theta;\rho)$, $u \equiv G_T(\theta;\rho)$.

$$G_T(\theta;\rho) \overset{(G.2)}{=} \begin{cases} \dfrac{4-3\pi^2\rho+\pi\rho(\theta+3\pi)}{8\pi}(\theta+\pi), & -\pi \le \theta < 0 \\ 0.5+\left[\dfrac{4+\pi^2\rho-\pi\rho\theta}{8\pi}\right]\theta, & 0 \le \theta \le \pi \end{cases} \Rightarrow$$

$$u \equiv \begin{cases} +\dfrac{\rho}{8}\theta^2+\dfrac{4+\pi^2\rho}{8\pi}\theta+\dfrac{1}{2}, & -\pi \le \theta < 0 \\ -\dfrac{\rho}{8}\theta^2+\dfrac{4+\pi^2\rho}{8\pi}\theta+\dfrac{1}{2}, & 0 \le \theta \le \pi \end{cases} \tag{I.1}$$

From (I.1), let $$a = \begin{cases} +\dfrac{\rho}{8}, & -\pi \le \theta < 0 \\ -\dfrac{\rho}{8}, & 0 \le \theta \le \pi \end{cases}, \quad b = \frac{4+\pi^2\rho}{8\pi}, \quad c = \frac{1}{2}-u. \tag{I.2}$$

Applying the quadratic solution of Press, Flannery, Teukolsky, and Vetterling (1986) for an accurate solution when *a*, *c*, or both are small (when $\rho \approx 0, u \approx 0.5$, the familiar quadratic solution $\theta = \left(-b \pm \sqrt{b^2-4ac}\right)/(2a)$ does not work),

$$q \overset{(I.2)}{\equiv} -\frac{1}{2}\left(b+\operatorname{sgn}(b)\sqrt{b^2-4ac}\right) = -\frac{1}{2}\left(b+\sqrt{b^2-4ac}\right) \Rightarrow$$

$$q = -\frac{1}{2}\left(b+\sqrt{b^2-4ac}\right) \tag{I.3}$$

$$\theta = \frac{c}{q} \tag{I.4}$$

Figure I-1, which was plotted with the following R code, verifies this result.

```
rho=.95*4/pi^2
u1 <-seq(0,.5,length=20)
a <- rho/8
b <- (4+pi^2*rho)/(8*pi)
c <- 0.5 - u1
q <- -.5*(b+sqrt(b^2-4*a*c))
x1 <- c/q

u2 <-seq(.5,1,length=20)
a <- -1*rho/8
b <- (4+pi^2*rho)/(8*pi)
c <- 0.5 - u2
q <- -.5*(b+sqrt(b^2-4*a*c))
x2 <- c/q

plot(c(u1,u2), c(x1,x2), ty="l")
```

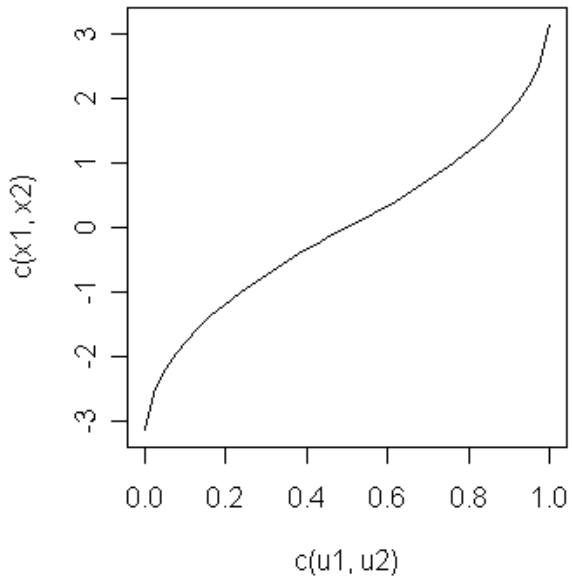

Figure I-1. Visual Verification of Triangular Inverse CDF, $\rho = 0.95 * 4/\pi^2$, Support $[-\pi, \pi)$ Radians.